Technology

Developmental Cell

Adeno-associated viral tools to trace neural development and connectivity across amphibians

Graphical abstract

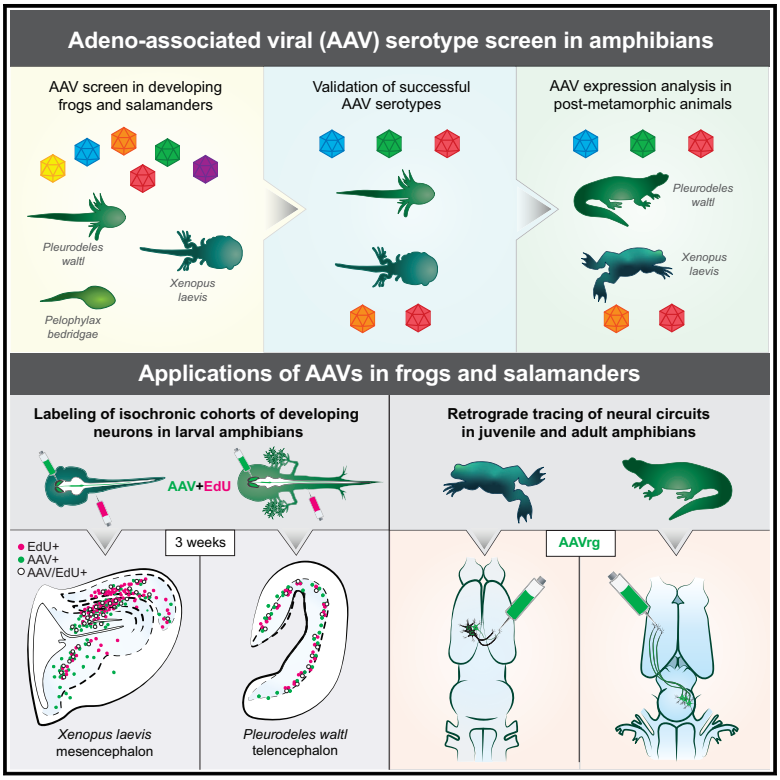

Highlights

- Scalable cross-species pipeline established for *in vivo* AAV serotype screening
- AAVs transduce amphibian neurons across CNS regions and developmental stages
- AAVs label isochronic cohorts of neurons in the developing amphibian CNS
- AAVs facilitate retrograde tracing of amphibian neural circuits

Authors

Eliza C.B. Jaeger, David Vijatovic, Astrid Deryckere, ..., Mark Shein-Idelson, Maria Antonietta Tosches, Lora B. Sweeney

Correspondence

mt3353@columbia.edu (M.A.T.), lora.sweeney@ist.ac.at (L.B.S.)

In brief

Jaeger et al. expand the toolkit for neuroscientists working on non-conventional animal species. The authors establish a screening strategy identifying adeno-associated viral vectors (AAVs) for three amphibian species and demonstrate that AAVs can deliver transgenes to the developing and mature CNS in both widespread and targeted manners.

Jaeger et al., 2025, Developmental Cell *60*, 1–19
March 10, 2025
https://doi.org/10.1016/j.devcel.2024.10.025

CellPress

Developmental Cell

CellPress
OPEN ACCESS

Technology

Adeno-associated viral tools to trace neural development and connectivity across amphibians

Eliza C.B. Jaeger,[1,8] David Vijatovic,[2,8] Astrid Deryckere,[1,8] Nikol Zorin,[3] Akemi L. Nguyen,[4] Georgiy Ivanian,[2] Jamie Woych,[1] Rebecca C. Arnold,[2] Alonso Ortega Gurrola,[1] Arik Shvartsman,[3] Francesca Barbieri,[2] Florina A. Toma,[2] Hollis T. Cline,[5] Timothy F. Shay,[6] Darcy B. Kelley,[1] Ayako Yamaguchi,[4] Mark Shein-Idelson,[3,7] Maria Antonietta Tosches,[1,9,*] and Lora B. Sweeney[2,9,10,*]

[1]Department of Biological Sciences, Columbia University, New York, NY, USA
[2]Institute of Science and Technology Austria, Klosterneuburg, Austria
[3]Department of Neurobiology, Biochemistry and Biophysics, Tel Aviv University, Tel Aviv, Israel
[4]Department of Biology, University of Utah, Salt Lake City, UT, USA
[5]Department of Neuroscience and Dorris Neuroscience Center, The Scripps Research Institute, La Jolla, CA, USA
[6]Division of Biology and Biological Engineering, California Institute of Technology, Pasadena, CA, USA
[7]Sagol School of Neuroscience, Tel Aviv University, Tel Aviv, Israel
[8]These authors contributed equally
[9]These authors contributed equally
[10]Lead contact
*Correspondence: mt3353@columbia.edu (M.A.T.), lora.sweeney@ist.ac.at (L.B.S.)
https://doi.org/10.1016/j.devcel.2024.10.025

SUMMARY

Amphibians, by virtue of their phylogenetic position, provide invaluable insights on nervous system evolution, development, and remodeling. The genetic toolkit for amphibians, however, remains limited. Recombinant adeno-associated viral vectors (AAVs) are a powerful alternative to transgenesis for labeling and manipulating neurons. Although successful in mammals, AAVs have never been shown to transduce amphibian cells efficiently. We screened AAVs in three amphibian species—the frogs *Xenopus laevis* and *Pelophylax bedriagae* and the salamander *Pleurodeles waltl*—and identified at least two AAV serotypes per species that transduce neurons. In developing amphibians, AAVs labeled groups of neurons generated at the same time during development. In the mature brain, AAVrg retrogradely traced long-range projections. Our study introduces AAVs as a tool for amphibian research, establishes a generalizable workflow for AAV screening in new species, and expands opportunities for cross-species comparisons of nervous system development, function, and evolution.

INTRODUCTION

Studies on amphibians have provided critical insight into the development, regeneration, function, and evolution of the vertebrate nervous system.[1–18] However, existing genetic tools to label and manipulate amphibian neurons have severe limitations. Transgenesis in amphibians is possible but slow due to amphibians' long generation time.[19–21] Electroporation can be used for the acute delivery of genes into amphibian cells, but it suffers from low efficacy and transient expression, with cell-type specificity additionally limited by the availability of *cis*-regulatory elements.[22,23] Direct injection of RNAs or morpholinos into developing frogs perturbs gene expression, but transiently and only at early developmental stages.[14,24] Viral vectors, by contrast, would offer an efficient and stable alternative that could be tailored to target cell types specifically.[25–27]

Recombinant adeno-associated viral vectors (AAVs) are well-suited for the study of the vertebrate nervous system.[25–27] As members of the Parvoviridae family, AAVs are single-stranded DNA dependoviruses that do not integrate into the host genome and can be rendered replication-deficient through genetic engineering.[28] They are widely used in mammalian neuroscience and gene therapy research, due to their ease of production, stable long-term expression, low immunogenicity, and minimal biosafety risks.[29–33] Tissue and cell-type selectivity of AAVs is conferred by natural or engineered variations in the capsid protein sequences,[34,35] enhancer-driven expression,[36–38] intersectional approaches,[29,37] or by targeting a specific developmental stage.[39,40] These advantages make AAVs an excellent tool to visualize, trace, and manipulate neural circuit connectivity and activity.

Here, we established a simple, scalable, and robust serotype screening strategy across three amphibian species (Figures 1A–1C), identifying efficient AAV serotypes for both frogs and salamanders. Using these serotypes, we introduce additional applications for AAVs in the developing and mature amphibian central nervous system (CNS). In larvae and tadpoles, we show that AAVs reproducibly transduce isochronic cohorts of neurons,

Please cite this article in press as: Jaeger et al., Adeno-associated viral tools to trace neural development and connectivity across amphibians, Developmental Cell (2024), https://doi.org/10.1016/j.devcel.2024.10.025

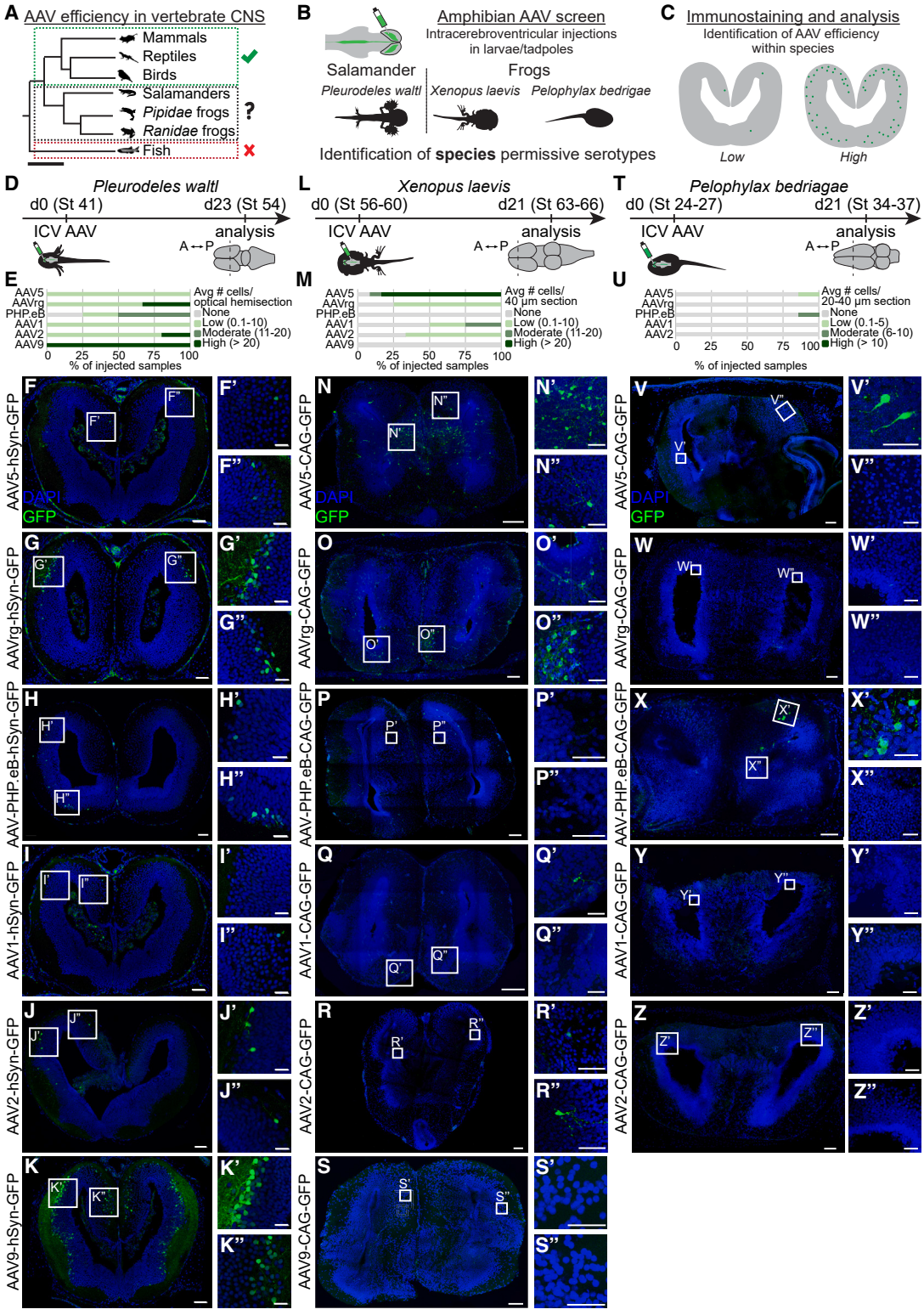

Figure 1. AAV serotype screen in *Pleurodeles*, *Xenopus*, and *Pelophylax* larvae

(A) Overview of AAV use in vertebrates. Check marks indicate successful CNS transduction of any AAV serotype, "x" indicates no CNS transduction with tested serotypes, and "?" indicates the need for further investigation. Scale bar represents 200 million years ago.

(B) Developing *Pleurodeles*, *Xenopus*, and *Pelophylax* were injected with a panel of AAV serotypes into the cerebral ventricle, enabling the identification of species-specific AAV expression patterns.

(legend continued on next page)

Please cite this article in press as: Jaeger et al., Adeno-associated viral tools to trace neural development and connectivity across amphibians, Developmental Cell (2024), https://doi.org/10.1016/j.devcel.2024.10.025

defined as groups of neurons that develop at the same time.[40] In post-metamorphic animals, we find that AAVs can be employed to either label neurons at the injection site or retrogradely trace axonal projections. These results open new opportunities to label and manipulate amphibian neural circuits and define a roadmap to optimize AAV tools in other vertebrate species.

DESIGN

Although viral vectors offer a promising strategy for the targeted delivery of genetic material to the nervous system, the vectors currently tested in amphibians have faced challenges. The use of rabies and pseudorabies viruses is restricted to short-term labeling because of high cytotoxicity.[41,42] Other viruses, such as vaccinia virus, adenoviruses, and vesicular stomatitis virus, transduce frog neurons, but their use is constrained by cytotoxicity, high biosafety level, and low availability.[43–45] In frogs, AAVs and lentiviruses have previously proven unreliable or ineffective.[44] In axolotls, foamy[46] and retroviruses[47] transduce only dividing cells, while vaccinia and pseudotyped baculoviruses infect postmitotic cells but are cytotoxic, cell type selective, and insufficiently available.[48] In other amphibian species, viral tools remain largely untested. To enable functional studies of the amphibian nervous system, we require a reliable toolkit to manipulate gene expression rapidly and with spatiotemporal control.

We designed a screen to identify AAV serotypes that infect amphibian neurons in two frog and one salamander species. The African clawed frog *Xenopus laevis*, the Levant water frog *Pelophylax bedriagae*, and the Iberian ribbed newt *Pleurodeles waltl* were selected based on their phylogenetic position (Figure 1A). The Anura (frogs) and Caudata (salamanders) orders diverged 272 million years ago, and together with Caecilians, represent the three orders of modern amphibians.[49,50] *Xenopus* and *Pelophylax* frogs, members of the Pipidae and Ranidae families, respectively, further diverged 182.5 million years ago.[49,50] The large phylogenetic distances between these species allow testing whether conserved principles of AAV tropism exist in amphibians.

Inspired by the widespread AAV uptake in the developing mouse brain,[40,51,52] we focused on early stages of amphibian development, when simple functional neural circuits coexist with neural progenitors and developing neurons that will populate adult circuits,[53] and animals are abundant and easy to maintain. AAVs were introduced via intracerebroventricular injections, an easy and minimally invasive method as brain ventricles are visible[54] and accessible at this stage. Intracerebroventricular virus administration caused broad spread across brain regions, increasing the probability of detecting labeled cells (Figure 1B). To make our screen more robust, we compared serotypes driving GFP expression and amplified the GFP signal by immunohistochemistry (Figure 1C). A broad panel of AAV serotypes—AAV1, AAV2, AAV5, AAV9, AAVrg, and AAV-PHP.eB—with distantly related capsid protein sequences[55] was selected to ensure coverage of AAV diversity. After the larval screen, the most promising serotypes were tested for neural transduction in post-metamorphic animals.

RESULTS

AAV serotype screen in the developing amphibian nervous system

In the salamander *P. waltl*, we injected AAV1, AAV2, AAV5, AAV9, AAVrg, or AAV-PHP.eB into the telencephalic ventricle of stage 41 larvae.[56] To restrict labeling to neurons, all AAV vectors initially tested expressed GFP under the control of the pan-neuronal human synapsin 1 (hSyn) promoter.[57] 3 weeks after injection, we evaluated the transduction efficiency of all serotypes (Figures 1D–1K; Table S1). In the injected hemisphere, we observed low labeling with AAV1, AAV5, AAV2, and AAVrg; moderate labeling with AAV-PHP.eB; and high labeling with AAV9. To test whether the ubiquitous CAG promoter[58] could increase expression strength, we compared CAG- and hSyn-driven expression using the AAV-PHP.eB serotype. While injection of AAV-PHP.eB-hSyn-GFP resulted in a low to moderate transduction, AAV-PHP.eB-CAG-GFP injection resulted in the highest levels of expression observed in this screen with labeling spanning the forebrain and midbrain (Figures S1A–S1M). GFP+ cells generally occupied a distinct layer of cells in the mantle zone of the pallium, which primarily includes neurons. The morphology of labeled cells was consistent with their neuronal nature: GFP labeled not only cell bodies but also dendrites and axonal tracts (Figures 1G, 1K, and S1C). These results indicate that several serotypes transduce neurons in developing salamanders, with AAV9, AAVrg, and AAV-PHP.eB (with CAG promoter) yielding the highest efficiency and reproducibility across biological replicates.

We next evaluated the transduction efficiency of AAV1, AAV2, AAV5, AAV9, AAVrg, and AAV-PHP.eB in the frog *X. laevis*. Prometamorphic tadpoles (NF stage 56–60)[59] were chosen for the primary screen since the brain organization and immune system at this stage are similar to juvenile and adult frogs.[60–62] Given the increased strength of CAG-driven AAV expression in *Pleurodeles*, the CAG promoter was used to drive GFP expression in *Xenopus*. 3 weeks after midbrain intracerebroventricular injection, we observed no GFP labeling with AAV9 and AAV-PHP.eB; low to moderate labeling with AAV1, AAV2, and AAVrg; and high labeling with AAV5 (Figures 1L–1S). AAV5-transduced cells were widespread throughout the telencephalon, diencephalon, mesencephalon, and rhombencephalon (Figures 1N, 2I, and S2B–S2E). To evaluate the robustness of the CAG promoter in *Xenopus*, we compared CAG- versus hSyn-driven AAV expression. For both promoters, AAV5 and AAVrg were the most efficient for brain transduction (Figures S1N–S1P and S1T), while

(C) 3 weeks after intracerebroventricular injection, brains were sectioned, GFP signal amplified, and transduction efficiency analyzed (D–Z) and scored per species as either absent, low, moderate, or high in its average expression (see STAR Methods).
(D–Z) For each serotype, left panels show representative overview images of coronal sections through the telencephalon, and right boxes indicate magnified regions. Scale bars in overview images and magnifications represent 100 and 40 μm, respectively. For each species, bar graphs represent the transduction efficiency of each serotype scored independently (E, M, and U).
Abbreviations: ICV, intracerebroventricular; St, stage.

Please cite this article in press as: Jaeger et al., Adeno-associated viral tools to trace neural development and connectivity across amphibians, Developmental Cell (2024), https://doi.org/10.1016/j.devcel.2024.10.025

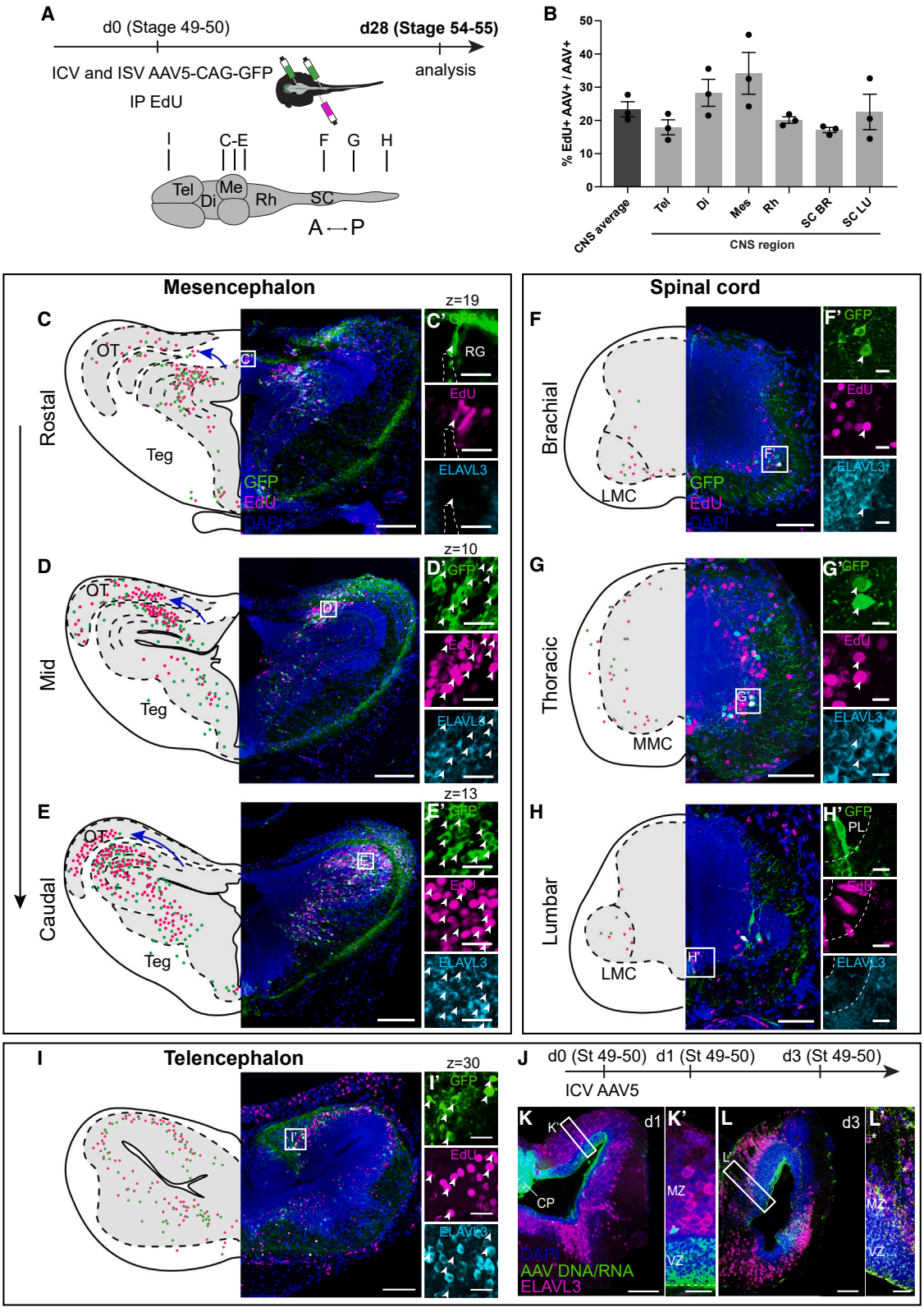

Figure 2. AAVs label distinct isochronic cohorts of neurons across the frog CNS

(A) Intracerebro- and intraspinoventricular injections of AAV5-CAG-GFP coupled with intraperitoneal injections of EdU in prometamorphic NF 49–50 *Xenopus* tadpoles. GFP and EdU signals were detected 3 to 4 weeks after injection.

(legend continued on next page)

Please cite this article in press as: Jaeger et al., Adeno-associated viral tools to trace neural development and connectivity across amphibians, Developmental Cell (2024), https://doi.org/10.1016/j.devcel.2024.10.025

AAV1, AAV2, and AAV9 were the least efficient (Figures S1Q–S1T). Co-staining with the neuron-specific marker Elavl3/4 (HuC/D)[63,64] demonstrated that the majority of labeled cells were neurons (Figures S1U–S1X). The CAG promoter drove higher expression levels than hSyn, with more brightly labeled soma and axons (Figures S1V and S1W), making it better suited for further AAV developmental and circuit tracing studies. We additionally screened AAVs in NF stage 40–41 tadpoles, finding that a similar panel of AAV serotypes, AAV1, AAV5, and AAVrg, transduces neurons across *Xenopus* development (Figures S1Y and S1Z). Finally, extending our analysis from the brain to the spinal cord, we demonstrated that central canal (intraspinoventricular) administration of AAV5-CAG-GFP at late metamorphic stages (NF stage 57–60; Figures S2G–S2K) labeled spinal neurons, highlighting this serotype's ability to label neurons across the CNS.

Lastly, we screened AAVs in wild-caught Levant water frogs, *P. bedriagae*, via intracerebroventricular injections at developmental larval stages 24–27 (Figures 1T–1Z).[65,66] AAV5 and AAV-PHP.eB injection produced sparse but clear GFP expression in the telencephalon (Figures 1V′ and 1X′). AAV5 injection led to more limited reporter gene expression than AAV-PHP.eB injection. No reporter gene expression was detected for AAVrg, AAV1, or AAV2. These results indicate that, while expression in *Pelophylax* tadpoles was sparse, AAVs can successfully infect telencephalic neurons across Anurans, even from wild-caught animals.

In summary, in *Pleurodeles*, *Xenopus*, and *Pelophylax*, we identified at least two serotypes per species that transduce neurons in the developing CNS, but observed differences in serotype specificity and transduction efficiency (Figures 1E, 1M, and 1U). In *Pleurodeles*, the best-performing serotypes were AAVrg, AAV-PHP.eB, and AAV9; in *Xenopus*, AAV5 and AAVrg; and in *Pelophylax*, AAV5 and AAV-PHP.eB.

AAVs target cohorts of developing neurons with temporal specificity

Intracerebroventricular administration of AAVs in both *Xenopus* tadpoles and *Pleurodeles* larvae resulted in reproducible labeling of specific cell clusters in examined brain regions (Figures 1 and S1). This observation motivated us to probe the rules and patterns of AAV transduction during CNS development. In the developing mouse entorhinal cortex and hippocampus, intracerebroventricular AAV injection labels isochronic cohorts of neurons—defined as groups of neurons that develop at the same time, mature synchronously, and assemble into distinct neural circuits.[40] We hypothesized that AAVs may target isochronic cohorts of neurons in developing amphibians as well, generating the reproducible patterns of GFP expression obtained after intracerebroventricular injections.

AAVs label isochronic cohorts of developing *X. laevis* neurons

Previous birthdating studies in *X. laevis* mapped when each brain region is generated during development.[53,67,68] This provided an ideal starting point to test whether AAVs are taken up specifically by developing neurons or their progenitors. We thus employed simultaneous intracerebroventricular or intraspinoventricular injection of AAV5-CAG-GFP and intraperitoneal injection of EdU[69,70] in premetamorphic NF 49–50 tadpoles (Figure 2A). 3 weeks later, we evaluated the number and distribution of EdU+, GFP+, and EdU+/GFP+ cells in the brain and spinal cord (Figures 2B–2I).

EdU labeling was pronounced in the mesencephalon (Figures 2C–2E), spinal cord (Figures 2F–2H), telencephalon (Figures 2I and S2B), and thalamus (Figures S2A–S2D), consistent with previous studies.[68,71–75] The spatial distribution of GFP+ cells largely matched the distribution of EdU+ cells (Figures 2C–2I and S2B–S2D). Across the CNS, ∼25% of transduced cells on average were also positive for EdU (Figure 2B). Other AAV-transduced cells, although not co-labeled by EdU, were intermingled with EdU+ cells. Conversely, regions such as the hypothalamus, which were largely EdU-negative and thus minimally proliferating at the time of injection (Figure S2C), were largely GFP-negative.

Within the mesencephalon, the EdU pattern closely followed the established course of optic tectum development,[75] with the medial addition of "wedges" of neurons that extend from the ventricular to the pial surface.[74,75] In the tectum, GFP and EdU labeling clustered into mediolateral and dorsoventral zones (Figures 2C–2E), suggesting that both neuron populations were born around the time of injection.

During frog metamorphosis, the spinal cord also undergoes extensive transformation with timed waves of neurogenesis yielding new molecularly and spatially distinct cell types.[53] To assess whether AAVs could access isochronic cohorts in the spinal cord, we injected AAV5-CAG-GFP intraspinoventricularly at early (NF 49–50), mid (NF 50–52) or late (NF 57) metamorphic

(B) Quantification of percentage of EdU+ AAV-transduced cells across the CNS (mean ± SEM, $n = 3$ tadpoles, all $p > 0.05$, one-way ANOVA).
(C–E) AAV and EdU signals overlap (white arrowheads) at the regional level at different rostral-caudal levels of the mesencephalon. Frog tectum expands medially and rostrally and then laterally and caudally (blue arrow). Transduced radial glia are GFP+ and EdU+ but not Elavl3+ (C′), whereas neurons are EdU+, GFP+, and Elavl3+ (D′ and E′).
(F–H) In the spinal cord, AAV labeling captures the expansion of either LMC motor neurons at limb levels (F and H) or of interneurons and MMC motor neurons at the thoracic level (G). AAV labels both neurons (F′ and G′) and radial glia cells (H′), many of which are also EdU-positive (white arrowheads).
(I) AAV and EdU signals in a coronal section through the telencephalon with many AAV+ EdU+ cells (white arrowheads).
Scale bars in overview images and magnifications represent 400 and 20 μm in (C)–(E) and 100 and 20 μm in (F)–(I), respectively. Images show maximum intensity projections of 40 μm z stacks except in (C′), (D′), (E′), (I′), (K), (K′), (L), and (L′) where a single z-plane is shown due to the large amounts of labeling.
(J–L) Prometamorphic tadpoles were injected intracerebroventricularly with AAV5-CAG-GFP and fixed 1 or 3 days after to inspect the viral DNA/RNA distribution using HCR. 1 day after injection (K), viral DNA/RNA was present in the CP and in the radial glia in the VZ but not in Elavl3+ neurons in the MZ (K′). 3 days after injection (L), the AAV DNA/RNA signal was present in the VZ and in radial glia processes (asterisks) (L′).
Abbreviations: BR, brachial; CP, choroid plexus; Di, diencephalon; IP, intraperitoneal injection; ISV, intraspinoventricular injection; LMC, lateral motor column; LU, lumbar; Me, mesencephalon; MMC, medial motor column; MZ, mantle zone; OT, optic tectum; PL, progenitor layer; RG, radial glia; Rh, rhombencephalon; SC, spinal cord; Teg, tegmentum; Tel, telencephalon; VZ, ventricular zone; see also Figure 1.

Please cite this article in press as: Jaeger et al., Adeno-associated viral tools to trace neural development and connectivity across amphibians, Developmental Cell (2024), https://doi.org/10.1016/j.devcel.2024.10.025

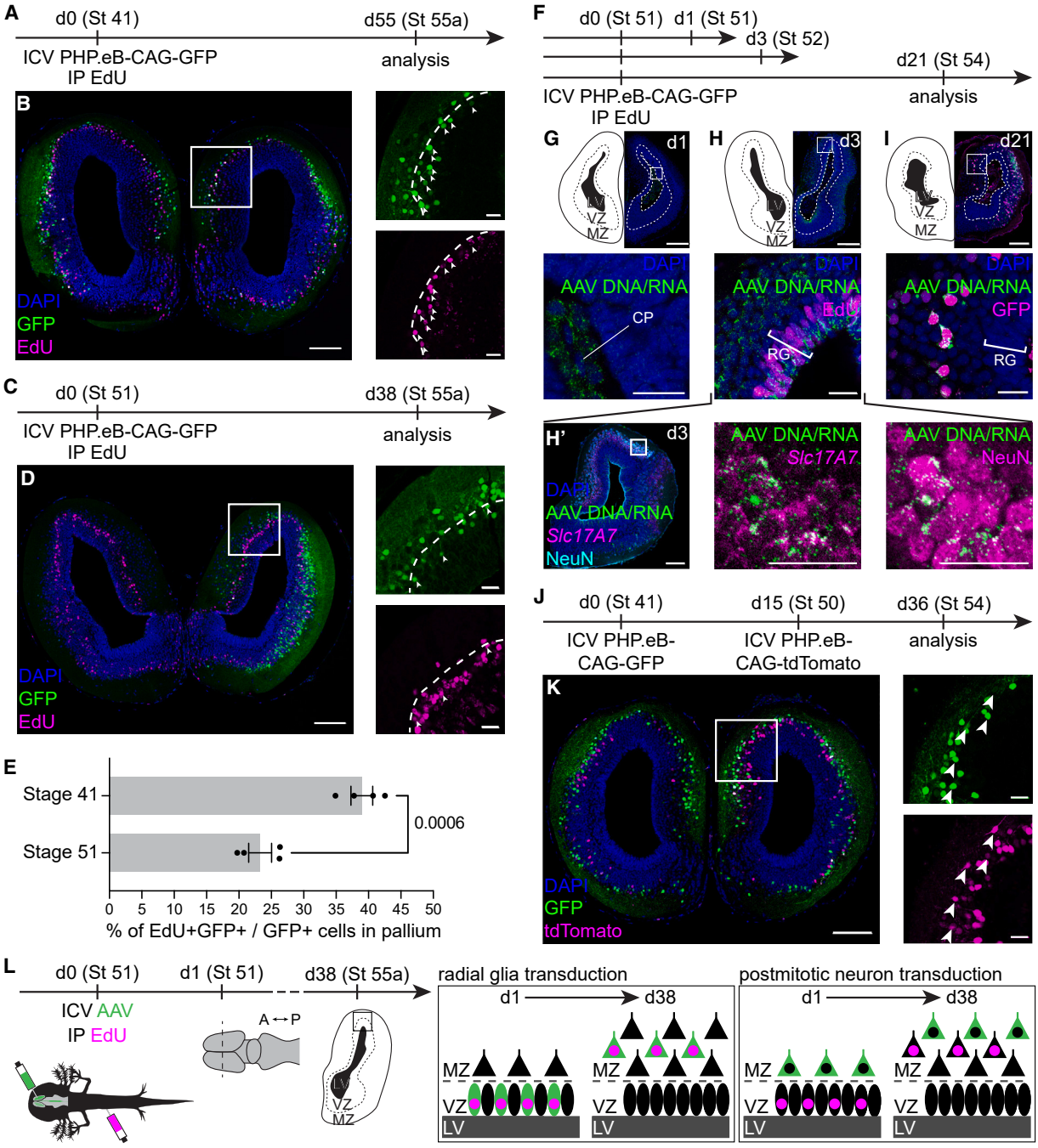

Figure 3. Labeling of different isochronic cohorts of neurons in the *Pleurodeles* telencephalon

(A–E) Experimental design showing injection of AAV-PHP.eB-CAG-GFP and EdU at early- (A) or late-active (C) *Pleurodeles* larval stages, visualization on a coronal section through the telencephalon in the pre-metamorphic larva (B and D), and quantification showing the percentage of EdU+ GFP+ cells over the total number of GFP+ cells in the pallium (E) (mean ± SEM, $n = 4$ larva per stage, $p = 0.0006$ by two-tailed unpaired t test). Boxes in (B) and (D) indicate magnified region, where arrowheads point toward double-labeled cells and dashed line to the leading edge of EdU+ cells.

(F) ICV injection of AAV-PHP.eB-CAG-GFP and IP injection of EdU in a late-active larva, and analysis 1, 3, or 21 days later.

(G–I) Coronal sections through the *Pleurodeles* telencephalon, showing presence of viral DNA/RNA in the choroid plexus at day 1 (G); viral DNA/RNA in radial glia lining the ventricle (EdU+) and neurons in the mantle zone of the telencephalon at day 3 (H); and viral DNA/RNA and GFP protein in neurons at day 21 (I). Boxes indicate magnified regions. (H′) Co-localization of viral DNA/RNA (green) with neuronal markers *Slc17A7* mRNA or NeuN protein at day 3.

(J) ICV injection of PHP.eB-CAG-GFP (St. 41) and PHP.eB-CAG-tdTomato (St. 50); analysis 21 days after the last injection.

(K) Coronal section through the *Pleurodeles* telencephalon showing GFP- and tdTomato-labeled cells. Box indicates the magnified region, where arrowheads point toward double-labeled cells. Scale bars in overview images and magnifications represent 200 and 40 μm, respectively.

(legend continued on next page)

Please cite this article in press as: Jaeger et al., Adeno-associated viral tools to trace neural development and connectivity across amphibians, Developmental Cell (2024), https://doi.org/10.1016/j.devcel.2024.10.025

stages. These injections resulted in labeling of the ventral (Figures 2F–2H), both ventral and dorsal (Figures S2E and S2F), or just dorsal spinal cord (Figures S2G and S2H), respectively.

Paired AAV5-CAG-GFP and EdU injections were then used to evaluate the relationship between AAV labeling and cell proliferation in the spinal cord. At the NF 49–50 stage, GFP and EdU both localized to the same spinal region (Figures 2F–2H). At brachial/lumbar limb-level segments, the majority of GFP+, EdU+, or co-labeled neurons were situated in the ventral horn and included lateral motor column neurons identified by their distinctive settling position and morphology (Figures 2F and 2H). At thoracic torso-level segments, AAV labeled mid-ventral interneurons and medial motor column motor neurons (Figure 2G).

In contrast to the intraspinoventricular injections at NF stage 57 (Figures S2G–S2J), direct injection of AAV into the spinal cord parenchyma at the same stage labeled motor neurons (Figures S2K and S2L), a postmitotic cell type born several stages earlier at NF 50–54.[71] This difference in the tropism based on delivery method indicates that ventricular administration of AAV is required to label spinal cord temporal cohorts, whereas intraparenchymal administration targets local and postmitotic neurons, as in mice.[39,40,76]

Across the CNS, in addition to neurons that were co-labeled with the Elavl3/4 marker (Figures 2D′–2G′, 2I′, S2B′, and S2C′), radial glia—identified by the absence of Elavl3/4 and presence of Sox2[68,77,78] expression, their elongated morphology, and their hallmark position in the progenitor zone—were sparsely labeled 3 weeks after AAV and EdU co-injections (Figures 2C′, 2H′, S2D′, and S2J′). Such radial glia labeling demonstrates that AAV5 can transduce and drive GFP expression in neural progenitors of both the *Xenopus* spinal cord and brain, suggesting that AAV uptake by radial glia underlies isochronic cohort labeling.

To directly test whether AAV5 transduces radial glia in *Xenopus* tadpoles, we used *in situ* hybridization chain reaction (HCR)[79] with probes for the viral genome and mRNA to detect AAV5-CAG-GFP uptake and expression (Figures 2J–2L). 1 day after injection, we detected AAV DNA/RNA signal in the choroid plexus and in radial glia cells in the ventricular zone but not in neurons within the mantle zone (labeled by Elavl3/4; Figures 2K and 2K′). A similar pattern was also visible 3 days after injection (Figure 2L). The radial glia identity of AAV-positive cells was confirmed by their cell body position, the absence of Elavl3/4 labeling (Figures 2K′ and 2L′), and the presence of AAV-positive glial processes spanning the ventricular, mantle, and marginal zones (Figure 2L′).

These findings indicate that intraventricular administration of AAV5 transduces radial glia in the *Xenopus* tadpole brain and spinal cord. Radial glia uptake of viral particles would then result in selective labeling of neurons born shortly after injection—when viral load is still high—consistent with AAV5 functioning as an isochronic cohort marker in *Xenopus*.

AAVs label isochronic cohorts of developing salamander neurons

Similar to *Xenopus*, we observed regionally restricted AAV labeling of neurons in the salamander brain: injection in the telencephalic ventricle of early active larvae (stage 41) resulted in the labeling of a superficial layer of neurons (Figures S1E–S1M). In *Xenopus*, pallial neurons are arranged at different distances from the ventricle according to their birthdate.[68] This layered distribution is ideal for studying cohorts of neurons generated at different developmental times.

To test whether AAV-PHP.eB labels neurons born around the time of injection in *Pleurodeles*, we combined intraperitoneal injection of EdU with intracerebroventricular injection of the AAV-PHP.eB virus (Figures 3A–3E). This dual injection resulted in the incorporation of both labels into neurons in premetamorphic larvae (stage 55a; Figure 3E). However, we observed a difference in the spatial distribution of these two labeled populations: GFP+ cells were further away from the ventricle than EdU+ cells (Figures 3B and 3D), suggesting that the virus transduced differentiated cells at the time of injection. This layered distribution of GFP+ and EdU+ cells was even more pronounced after dual injection at stage 51, when there are more differentiated neurons than at stage 41 (Figures 3C–3E), providing further support for direct neuronal transduction.

To directly test whether AAV-PHP.eB transduces radial glia or postmitotic neurons in *Pleurodeles*, we examined viral DNA/RNA using HCR (Figure 3F). 1 day after injection, we detected AAV DNA/RNA in the choroid plexus,[80] as in *Xenopus* (Figure 3G). Unlike in *Xenopus*, however, the virus was not detected in radial glia cells at this stage. By contrast, 3 days after injection, viral DNA/RNA was present in both EdU+ radial glia in the ventricular zone and in neurons in the mantle zone (Figure 3H). The colocalization of viral DNA/RNA with *Slc17A7* mRNA, a marker of excitatory neurons,[81,82] and NeuN, expressed in differentiated neurons[83] (Figure 3H′), combined with the absence of EdU signal in the mantle zone (Figure 3H), indicated that neurons transduced by AAV-PHP.eB were already postmitotic at the time of AAV injection. 3 weeks after injection, viral DNA/RNA and GFP protein co-labeling was restricted to neurons and not detected in radial glia cells (Figure 3I).

Next, we asked whether AAVs injected in the telencephalic ventricle at a certain developmental time point transduce every neuron at the time of injection or only a specific subset. Sequential injections of AAV-PHP.eB expressing GFP at early stages (stage 41) and AAV-PHP.eB expressing tdTomato at late-active larval stages (stage 50) labeled largely distinct cohorts of neurons (Figures 3J and 3K). Labeled neurons were distributed according to the outside-in sequence of neurogenesis[68]: GFP+ neurons were generally more superficial than tdTomato+ neurons. This indicates that intracerebroventricular AAV injections do not label neurons indiscriminately but instead target neurons within a certain distance from the ventricle.

The ability of AAVs to label cohorts of neurons after intracerebroventricular injections into developing larvae can be explained

(L) Schematic overview of two mechanisms of viral labeling. ICV injection of AAVs can lead to transduction of proliferating radial glia in the VZ, which would also incorporate EdU if in S phase (left), or transduction of differentiated neurons in the MZ (right). 3 weeks after injection, this would result in labeling of either EdU+ GFP+ neurons (left) or differential neuronal labeling (right).
Abbreviations: LV, lateral ventricle; see also Figures 1 and 2.

Please cite this article in press as: Jaeger et al., Adeno-associated viral tools to trace neural development and connectivity across amphibians, Developmental Cell (2024), https://doi.org/10.1016/j.devcel.2024.10.025

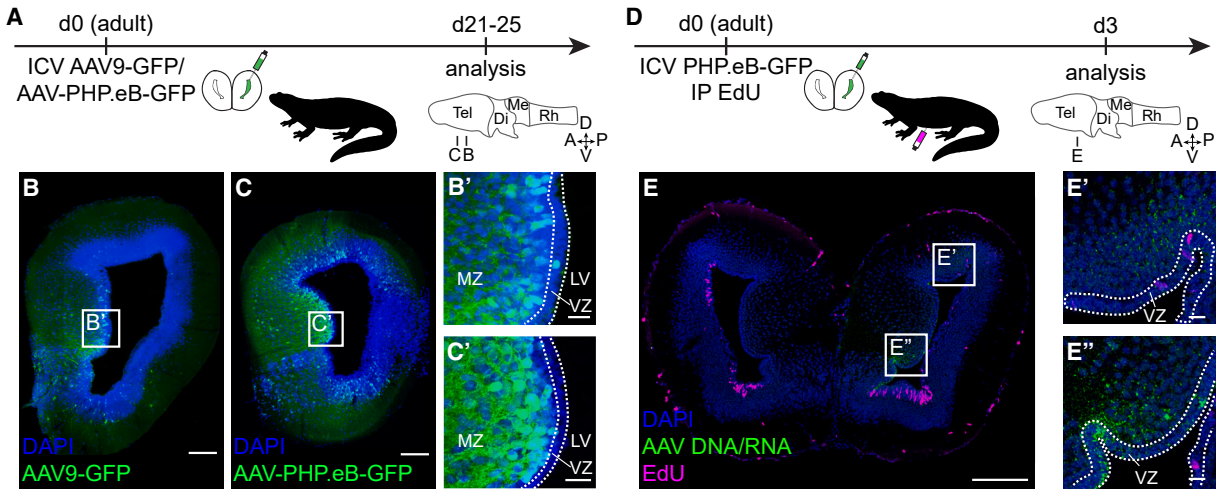

Figure 4. Intracerebroventricular AAV injections produce widespread labeling of neurons but not ependymoglia in the post-metamorphic *Pleurodeles* telencephalon

(A) Experimental design.

(B and C) Coronal sections through the *Pleurodeles* telencephalon showing GFP labeled cells in 152- and 105-day-old post-metamorphic animals injected with AAV9-CAG-GFP (B) or AAV-PHP.eB-CAG-GFP (C), respectively. Boxes indicate magnified regions (B′ and C′). Both viruses transduce neurons throughout the MZ, with limited transduction of ependymoglia in the VZ.

(D) Experimental design: ICV injection of PHP.eB-CAG-GFP and IP injection of EdU in a post-metamorphic animal (133 days old), and analysis 3 days later.

(E) At day 3, viral DNA/RNA is present in both ependymoglial cells lining the ventricle and neurons in the telencephalic MZ. Viral transduction is not correlated with cell proliferation, as indicated by the lack of overlap with EdU. Boxes indicate magnified regions (E′ and E″). Scale bars in overview images and magnifications represent 200 and 40 μm, respectively.

Abbreviations: Di, diencephalon; Rh, rhombencephalon; see also Figures 1, 2, and 3.

by two different mechanisms (Figure 3L). AAVs could transduce neural progenitors—the radial glia cells located at the ventricle—with only cells in their last cell cycle (i.e., future neurons) retaining enough viral payload for detectable GFP expression 3 weeks later ("radial glia transduction," Figure 3L). Alternatively, AAVs injected in the ventricle could transduce neurons already postmitotic at the time of injection, with these neurons pushed further away from the ventricle by neurons generated later in development ("postmitotic neuron transduction," Figure 3L). Our experiments indicate that AAV5 transduction in *Xenopus* primarily follows the first mechanism, whereas AAV-PHP.eB in *Pleurodeles* uses a combination of radial glia and neuronal transduction but results in payload expression only in neurons. The transduction of both neural progenitors and postmitotic neurons in *Pleurodeles* also shows that AAV-PHP.eB and EdU cannot be used interchangeably for birthdating studies in this species.

Transient detection of AAV DNA/RNA (Figure 3H) but not GFP protein (Figure 3I) in *Pleurodeles'* radial glia indicates that viral genomes are either diluted rapidly during cell proliferation or that AAV payload transcription or translation are impaired specifically in this cell type.[84] To distinguish between these two possibilities, we performed intracerebroventricular AAV injections in post-metamorphic juveniles (stage 56),[56] in which the majority of radial glia cells have transitioned to quiescence and are called ependymoglial cells[12] (EGCs). EGCs re-enter a proliferative state after brain and spinal cord injury, fueling the regeneration of these tissues.[7,8,85–87] Injections of AAV9-CAG-GFP or AAV-PHP.eB-CAG-GFP into the telencephalic ventricle of post-metamorphic animals produced neuronal labeling along the entire rostrocaudal axis of the injected hemisphere (Figures 4A–4C and S3A–S3H), indicating direct transduction of differentiated neurons. Neuronal transduction was confirmed by AAV DNA/RNA signal in neurons in the mantle zone, already postmitotic at the time of injection, as indicated by a lack of EdU uptake (Figures 4D and 4E). In post-metamorphic animals, AAV9 and AAV-PHP.eB intracerebroventricular injections also resulted in broad AAV DNA/RNA signal in EGCs but extremely sparse GFP protein expression (Figure 4) in line with results in larvae (Figure 3H). Given that EGCs can be labeled by direct electroporation of plasmids with the CAG promoter (Figures S3K and S3L), the lack of AAV-driven GFP expression suggests cell-type-specific repression of viral payload expression[88] in EGCs.

In sum, intracerebroventricular AAV injections in *Pleurodeles* result in the labeling of isochronic cohorts of neurons in larvae and widespread transduction of neurons in post-metamorphic juveniles. Although the virus transduces radial glia cells and EGCs in *Pleurodeles*, expression of the viral payload in these cell types and this species is impaired after viral entry.

AAVs transduce neurons in post-metamorphic amphibians

We next asked whether AAV serotypes that infect the larval nervous system by intraventricular injection also infect the post-metamorphic (juvenile and adult) nervous system by intraparenchymal injection, enabling targeting of neurons with tight spatial control. First, we injected the two most efficient AAV serotypes from our *Xenopus* tadpole screen—AAV5 and AAVrg—into the medial and dorsal pallium of juvenile (Figures 5A–5D; Table S2; post-metamorphic stages 0–5[89]) and sexually mature adult frogs (Figures 5E–5H; Table S2). At both juvenile and adult stages,

Please cite this article in press as: Jaeger et al., Adeno-associated viral tools to trace neural development and connectivity across amphibians, Developmental Cell (2024), https://doi.org/10.1016/j.devcel.2024.10.025

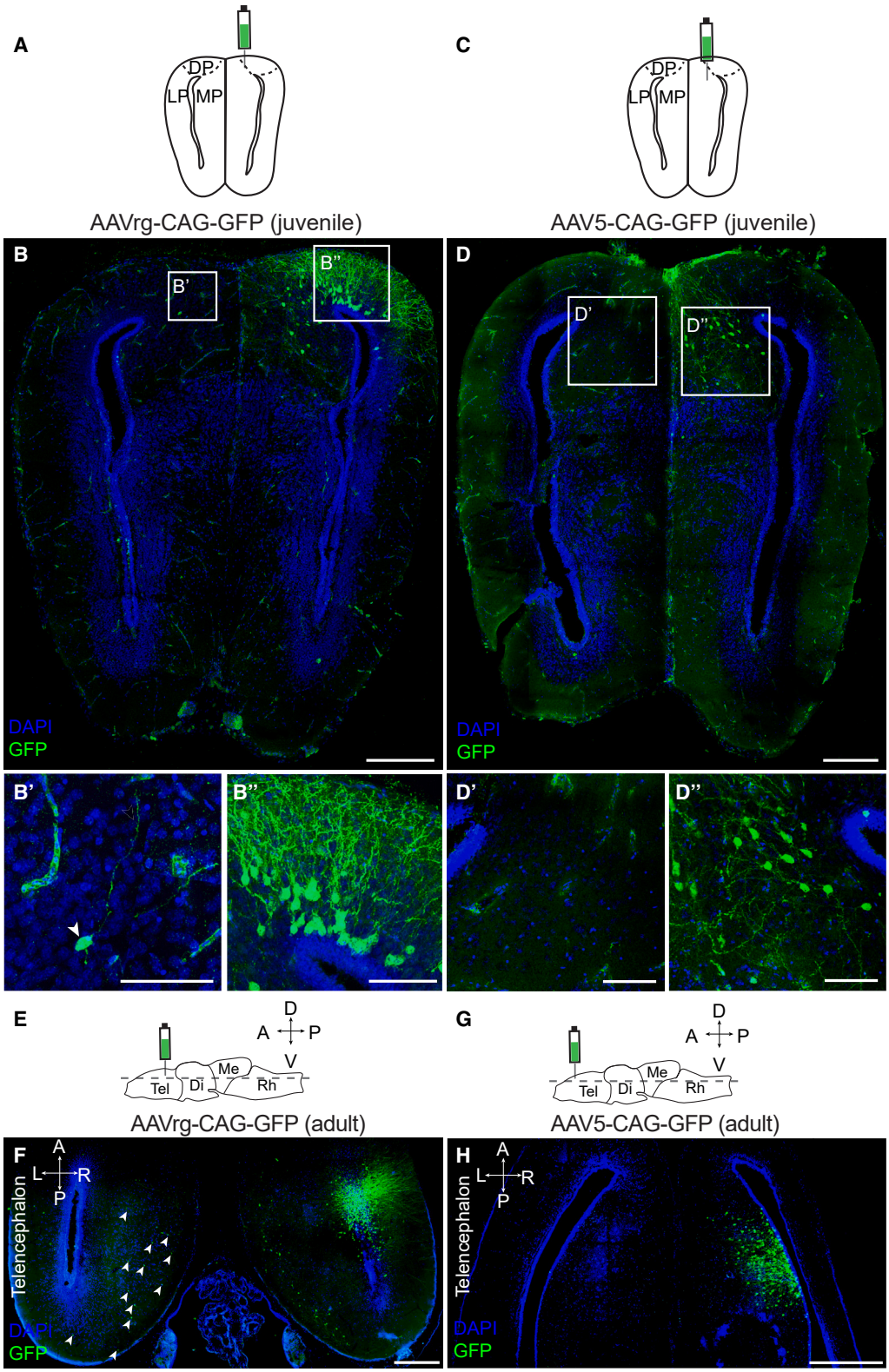

Figure 5. AAVrg and AAV5 transduce neurons in *Xenopus* juveniles and adults

(A–D) Coronal section through the juvenile *Xenopus* telencephalon 3 weeks after AAVrg-CAG-GFP (A and B), or AAV5-CAG-GFP (C and D) direct injection into the medial-dorsal pallium, or medial pallium, respectively. AAVrg sparsely labeled neurons in the contralateral pallium (B′) and strongly labeled neurons in the ipsilateral pallium (B″). AAV5 labeled only ipsilateral neurons in juvenile frogs (D).

(legend continued on next page)

Please cite this article in press as: Jaeger et al., Adeno-associated viral tools to trace neural development and connectivity across amphibians, Developmental Cell (2024), https://doi.org/10.1016/j.devcel.2024.10.025

AAV5 and AAVrg transduced neurons around the injection site (Figures 5A–5H).

To determine whether AAVs similarly transduce post-metamorphic juvenile and adult *Pleurodeles*, we directly injected AAVs into dorsal pallium parenchyma. Injections of AAV9, AAV-PHP.eB, and AAVrg resulted in GFP expression around the injection site (Figure 6), while AAV1 and AAV5 injections did not produce any labeling (Figures S4A and S4B; Table S1). The position and morphology of labeled cells indicated that these viral vectors transduced neurons, characterized by numerous apical dendrites extending toward the pial surface.[90] In *Pleurodeles*, the results of intraparenchymal injection in post-metamorphic animals were different from the outcomes of intracerebroventricular injections (Figures 4B and 4C). Intracerebroventricular injections produced neuronal labeling extending ~3 mm along the rostrocaudal axis (Figures S3A–S3H), whereas intraparenchymal AAV injections resulted in spatially restricted GFP expression, limited to ~300–600 μm around the injection site (Figures 6A–6U). Different injection strategies can therefore produce either spatially restricted or widespread rostrocaudal labeling in post-metamorphic salamanders.

Unlike AAV injections in larval *Pleurodeles*, which generally resulted in consistent transduction efficiency across individuals, AAV injections in post-metamorphic animals yielded variable results, ranging from hundreds of labeled neurons in some animals to no labeling in others (Table S3). We sought to identify the sources of this variability, one of which could be the strength of the promoter driving GFP expression. Direct comparisons of AAV9-CAG-GFP and AAV9-hSyn-GFP expression after intraparenchymal injection showed that CAG drove higher expression levels in neurons in post-metamorphic animals (Figure S4C). However, even though the hSyn promoter was weaker, we could still detect GFP-expressing neurons around the injection site using immunostaining for GFP. A comparison of GFP detection with and without immunolabeling confirmed that GFP signal amplification is critical to detect transduced neurons when the endogenous fluorescence is weak (Figures S4D–S4F). These results indicate that promoter choice altered the level of expression but not our ability to detect transduced neurons and thus could not fully explain the variation we observed.

To query other sources of variation, we analyzed metadata and injection outcomes for additional 68 intraparenchymal injections performed in 39 post-metamorphic *Pleurodeles* salamanders. This dataset included both quantitative variables (age, weight, viral genomes injected, and transduction score; see STAR Methods) and categorical variables (serotype, promoter, reporter, single versus dual injection, manufacturer, and injection site). To assess the associations between these variables, we performed a factor analysis for mixed data (FAMD), a principal component method that is designed to determine significant sources of variability within datasets that contain both quantitative and qualitative data types (Figures 6V–6Y and S4G–S4V).[91]

As expected, variables including reporter, serotype, and promoter contributed significantly to the variability in the dataset (Figure S4L). FAMD also indicated that animal age and weight significantly contributed to variability above chance (Figure S4L). Linear regression of age against expression score within this dataset confirmed a negative correlation between animal age and transduction efficiency (Figure S4G). Animal weight, which generally increases with age, also had a negative correlation with expression score (Figure S4H). These results suggest that AAV transduction efficiency in post-metamorphic salamander brains declines with increasing animal age and size.

Finally, we assessed neuronal transduction in wild-caught adult *P. bedriagae* frogs. As intracerebroventricular injections into neonatal mice[92] and juvenile salamanders (Figures 4A–4C and S3A–S3H) produced widespread labeling of mature neurons in the brain, we applied a similar injection method in *Pelophylax*. However, intracerebroventricular injection of AAV5, AAVrg, or AAV-PHP.eB into the *Pelophylax* telencephalon did not produce any GFP expression (Table S1).

Retrograde axonal tracing with AAVrg in frogs and salamanders

Of all serotypes screened, only AAVrg, an engineered serotype transported retrogradely along axons in mice,[93] efficiently transduced neurons in both *Xenopus* frogs and salamanders. We thus determined whether AAVrg also functions as a retrograde tracer in amphibians.

First, we compared the results of direct AAVrg injections in *Xenopus* with previous knowledge of frog pallial connectivity. Neurons in the frog pallium have extensive ipsilateral and sparse contralateral projections[94,95]; therefore, after AAV5 or AAVrg intraparenchymal injection, we scored ipsilateral and contralateral pallial labeling in juvenile frogs (Figures 7A, 7B, and S5). Direct injection of AAV5-CAG-GFP in the pallium exclusively labeled ipsilateral neurons with ~1 mm of rostrocaudal spread (Figures 7A and 7B). By contrast, AAVrg-CAG-GFP injection, which also resulted in expression restricted to the telencephalon, labeled neurons in both the ipsilateral and contralateral hemispheres and axons in the hippocampal commissure with a broader ~2 mm rostrocaudal spread ipsilaterally (Figures 7B–7F and S5), indicating retrograde transport of AAVrg within the *Xenopus* CNS.

To test AAVrg-dependent retrograde labeling in salamanders, we co-injected AAVrg-hSyn-GFP and AAV-PHP.eB-CAG-tdTomato into the pallium of post-metamorphic *Pleurodeles*. 3 weeks post injection, AAV-PHP.eB-driven tdTomato-expressing cells were found exclusively around the injection site (Figures 7H and 7I). By contrast, AAVrg-driven GFP expression was more widespread, with GFP+ neuronal cell bodies around the injection site and GFP+ axonal tracts in the ipsilateral and contralateral striatal neuropil and lateral forebrain bundle (Figures 7J–7L). GFP+ axons were also visible in the anterior and hippocampal commissures (Figure 7L), diencephalon, and midbrain. In the midbrain, GFP-expressing neuronal cell bodies were observed in multiple areas about 4 mm away from the injection site (Figures 7M and S6). The pattern of GFP expression

(E–H) Horizontal sections through the adult *Xenopus* telencephalon 3 weeks after AAVrg-CAG-GFP (F) or AAV5-CAG-GFP (H) direct injection into the telencephalon. AAVrg labeled both ipsilateral and contralateral neurons (white arrows in F). AAV5 labeled only ipsilateral neurons (H). Scale bars in overview images and magnifications represent 400 and 50 μm, respectively.

Abbreviations: DP, dorsal pallium; L, left; LP, lateral pallium; MP, medial pallium; see also Figures 1, 2, 3, and 4.

Please cite this article in press as: Jaeger et al., Adeno-associated viral tools to trace neural development and connectivity across amphibians, Developmental Cell (2024), https://doi.org/10.1016/j.devcel.2024.10.025

CellPress
OPEN ACCESS

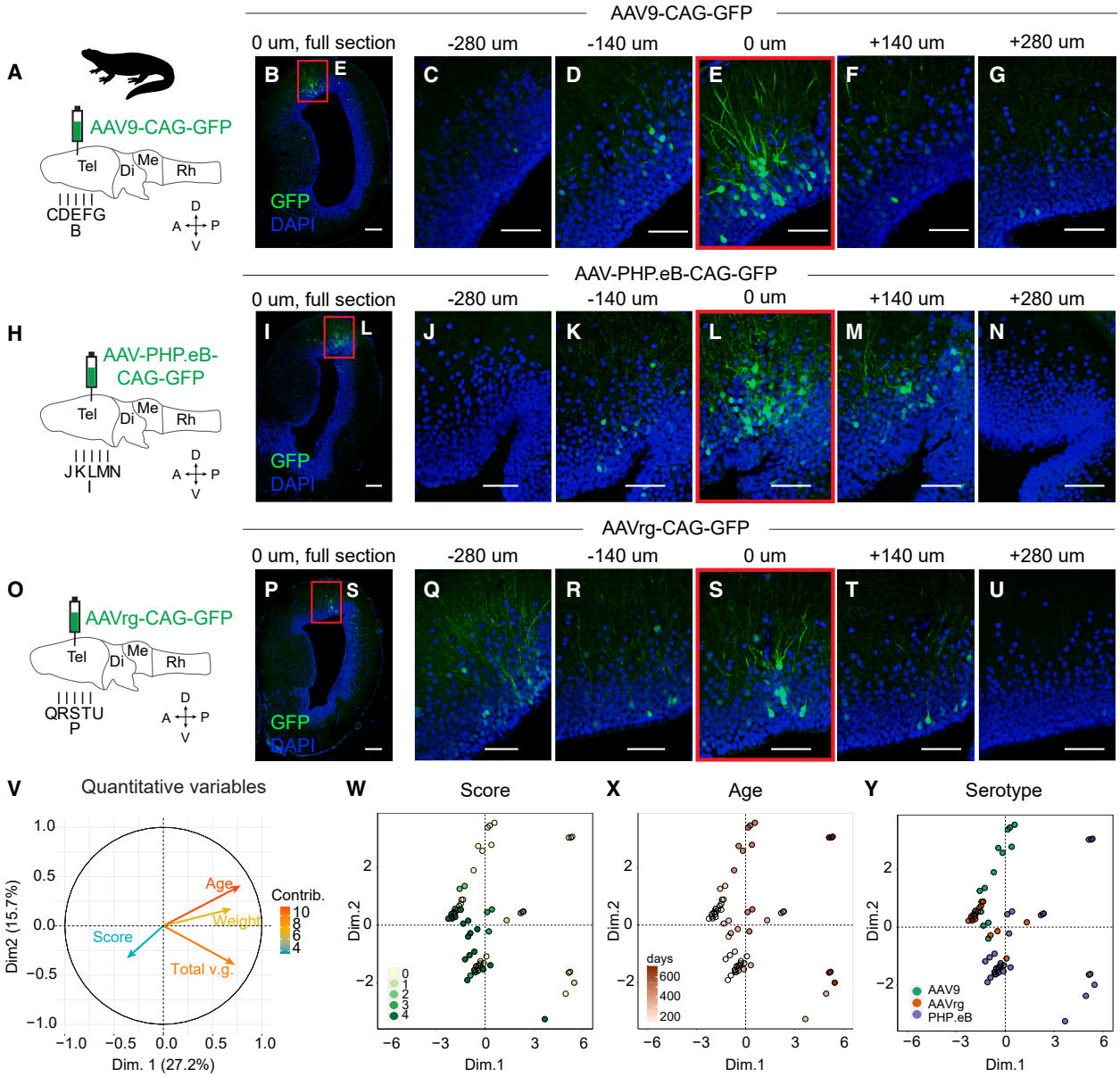

Figure 6. AAV serotype screen in post-metamorphic *Pleurodeles*

(A–U) Direct intrapallial injections of AAV9-CAG-GFP (A–G), AAV-PHP.eB-CAG-GFP (H–N), or AAVrg-CAG-GFP (O–U) in post-metamorphic animals 230, 280, or 319 days old, respectively. (A, H, and O) Schematics indicate the injection site and section planes. (B, I, and P) GFP-expressing neurons around the injection site, with red boxes indicating the magnified region at the injection level, and magnifications of sequential sections are 140 μm apart. Distance from the injection site (0 μm) is shown. Scale bars in overview images and magnifications represent 200 and 100 μm, respectively.

(V) Correlation circle of all quantitative variables contributing to injection outcome variability, quantified using factor analysis for mixed data (FAMD). Stronger contributions to the first two dimensions are indicated by hotter line and text color. Both quantitative and qualitative variables were analyzed for their contributions to overall variability across 68 injection outcomes (see STAR Methods for analysis and scoring criteria).

(W–Y) Individual injections are represented by filled dots, plotted across FAMD Dim. 1 and Dim. 2. and colored according to score, age, and serotype. See Figure S4 and Table S3 for the full dataset included in FAMD and additional plots.

Abbreviations: see Figures 1–5.

indicates that AAVrg was taken up by axonal terminals at the injection site and traveled retrogradely to reach dorsal pallium-projecting neurons in the midbrain. These findings not only show that AAVrg works as a retrograde tracer in salamanders, but also corroborate the existence of direct projections from the midbrain to the pallium in amphibians, as described previously with dye-based tracing.[18,96]

Our results thus demonstrate that AAVrg is a powerful viral tool for neuronal labeling and axonal tracing in both frogs and salamanders.

Please cite this article in press as: Jaeger et al., Adeno-associated viral tools to trace neural development and connectivity across amphibians, Developmental Cell (2024), https://doi.org/10.1016/j.devcel.2024.10.025

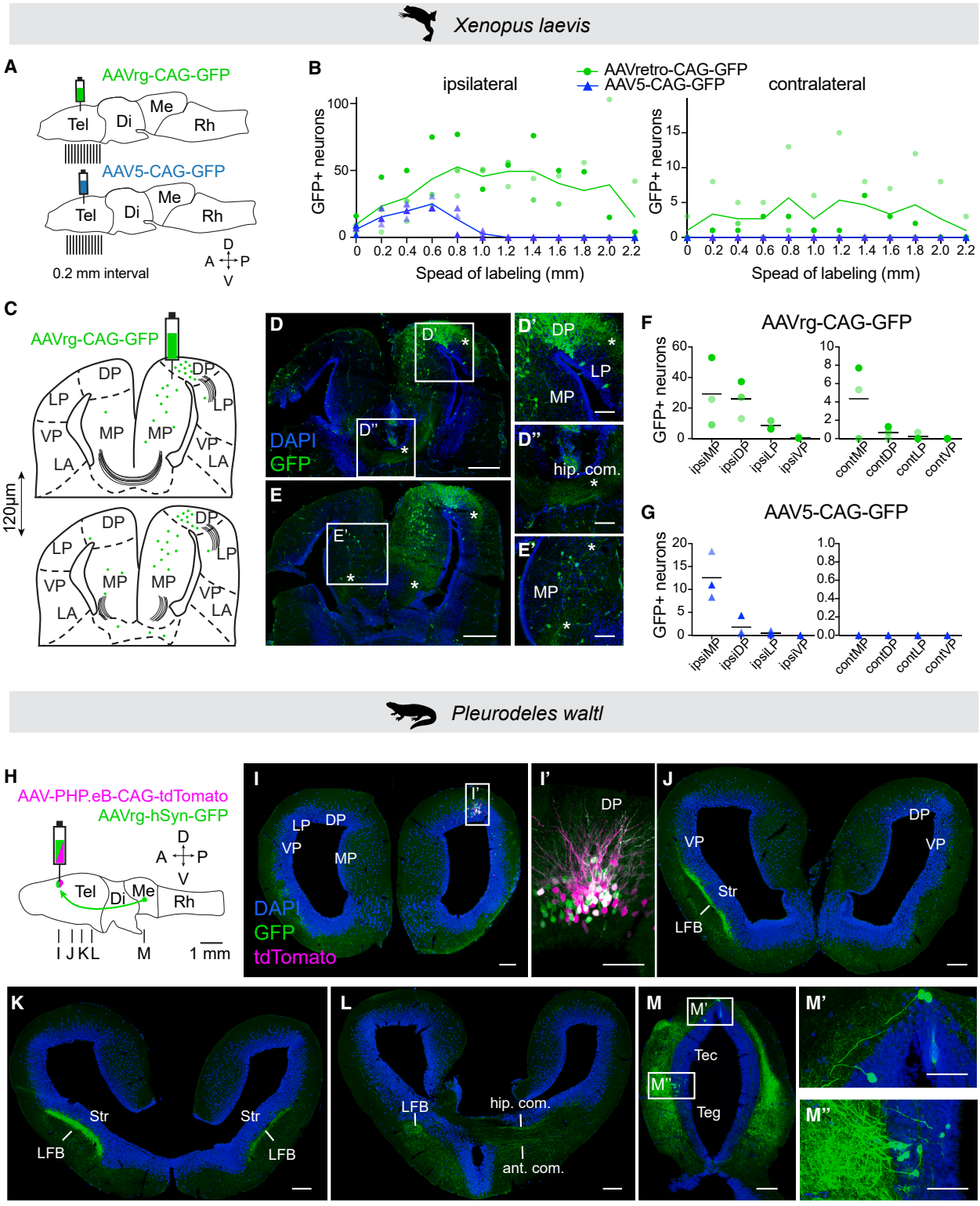

Figure 7. Retrograde tracing of neural circuits with AAVrg in *Xenopus* and *Pleurodeles*

(A) Schematics showing injection sites and section planes for analysis of AAVrg-CAG-GFP and AAV5-CAG-GFP spread after injection into medial-dorsal pallium of juvenile *Xenopus*.

(B) The numbers of labeled soma across the anteroposterior axis on the ipsilateral (left) and contralateral side (right) for AAVrg (green, $n = 3$) and AAV5 (blue, $n = 3$), and different color shades represent individual replicates.

(legend continued on next page)

Please cite this article in press as: Jaeger et al., Adeno-associated viral tools to trace neural development and connectivity across amphibians, Developmental Cell (2024), https://doi.org/10.1016/j.devcel.2024.10.025

DISCUSSION

AAV vectors, despite having significant potential for species not amenable to transgenesis, have only recently been employed in non-human primates,[97,98] birds,[99–102] and reptiles.[103] Previous experiments in zebrafish[104] and frogs[44] resulted in little to no AAV transduction of the brain. Here, we demonstrate that AAVs infect the CNS of three distantly related species of amphibians. Our findings provide a roadmap for screening AAVs in new species, reveal aspects of AAV biology, and expand neuroscience research opportunities for amphibian species.

Screening the AAV toolbox in new vertebrate species

Four key elements of our experimental design proved essential for the success of our AAV screen. First, we started from a broad set of serotypes, without assuming that a serotype that works well in one amphibian species would work in others. Indeed, none of the serotypes screened produced high transduction in all three amphibian species. Serotype efficiency in a new species cannot be predicted from other species: AAV tropism is similar in the two salamanders *Pleurodeles* and axolotl (see recent findings by Lust and Tanaka[105]) but markedly different in the two frogs *Xenopus* and *Pelophylax*. We thus conclude that an unbiased set of AAV serotypes is the ideal starting point for screening new species. Second, the delivery strategy matters. We observed distinct populations of neurons labeled by intraventricular versus intraparenchymal injection. The speed and volume of our intraparenchymal injections in adults differed markedly from previous experiments in frogs,[44] indicating slow and low-volume virus delivery is essential for successful transduction. Third, our ability to detect transduced neurons was enhanced by a strong and ubiquitous promoter and by immunohistochemical signal amplification. Finally, we found that AAVs that efficiently transduce tissue during one stage of development generally work also at other developmental stages, including post-metamorphic juveniles and adults. Older post-metamorphic *Pleurodeles* proved the exception: transduction efficiency decreased with age. This motivates a two-tiered screening design: first target developing animals and then verify if the top candidates also transduce adult animals.

Lessons on AAV biology from amphibians

Our experiments in amphibians also suggest new aspects of AAV biology, informing the design and optimization of AAV vectors as tools for gene delivery in new organisms.

The lack of demonstrated success of AAVs in aquatic vertebrates[104] until now suggested that AAV vectors were functional only in terrestrial animals or in endotherms. Indeed, all commercially available vectors are derived from viruses that have mammals as natural hosts.[29] However, our experiments show that AAV transduction is efficient also in aquatic ectotherms living at temperatures lower than 37°C. Body temperature is thus not a limiting factor for the application of mammalian-derived AAV vectors to vertebrate species, raising the potential that further testing in other aquatic species, such as fish,[104] may be warranted.

Our comparisons between species, life stages, and cell types revealed differences between AAV serotypes that may depend on different mechanisms for viral uptake and expression. Each serotype binds to a specific combination of cell surface glycans and protein receptors for cellular transduction.[106] Both AAV-PHP.eB and its parent virus AAV9, which in mammals use GPR108 for cell entry and intracellular trafficking,[107] worked in *Pleurodeles* but not in *Xenopus*. Conversely, AAV5, the most distantly related to all other AAV serotypes,[108] was the most efficient virus in *Xenopus* and among the least efficient in *Pleurodeles*. In mammals, AAV5 is notably GPR108-independent.[109,110] In frog genomes, there is no evidence for the GPR108 receptor.[111,112] Thus, the absence of this receptor may indicate why AAV5, and not AAV9 or AAV-PHP.eB is the most successful frog serotype. In birds, which also lack GPR108, overexpression of this receptor boosts AAV transduction.[113]

After AAV cell entry, interactions between viral particles and intracellular machinery are crucial for successful payload expression. Some of these interactions might be cell-type specific, determining AAV cellular tropism. In *Pleurodeles*, AAV-PHP.eB drives protein expression in neurons but fails to express protein in radial glia and EGCs, even though viral nucleic acids are detected in these cell types. Radial glia and EGCs are most closely related to mammalian astrocytes, which are transduced by AAV-PHP.eB with high efficiency.[114] Differences in AAV tropism across species thus may depend not only on the evolutionary divergence of cell surface receptors,[113] but also

(C–E) Schematic of two coronal sections from the same brain, with labeled cells (green dots) and commissures (black lines) after injection of AAVrg-CAG-GFP into MP/DP (C), observed on coronal sections (D and E). Asterisks mark axons to the LP (D′), axonal tracts of the hippocampal commissure (D″), and traced axons in the contralateral MP (E′).

(F and G) Quantification of GFP-positive cells in distinct telencephalic areas after injection of AAVrg-CAG-GFP (F) or AAV5-CAG-GFP (G), and each dot represents an animal marked by a different shade of green (AAVrg) or blue (AAV5). Contralateral labeling was compared between AAV5 and AAVrg for each region (mean, n = 3 juveniles, Kruskal-Wallis followed by a Dunn's multiple comparison test: p = 0.08, 0.18, and >0.999 for contMP, contDP, and contLP, respectively). For *Xenopus*, scale bars in overview image and magnifications represent 400 and 50 μm, respectively. For an additional example, see Figure S5.

(H) Schematic showing injection site and section planes for the co-injection of AAV-PHP.eB-CAG-tdTomato and AAVrg-hSyn-GFP in the DP of a post-metamorphic *Pleurodeles*. Arrow indicates axonal projections to DP from the midbrain.

(I) Coronal section showing both tdTomato and GFP labeling at the injection site. (I′) Maximum intensity projection of a 25 μm stack of 5 images taken at 5 μm intervals at the injection site.

(J–L) Representative coronal sections along the anterior-posterior axis showing GFP expression far from the injection site, including strong axonal expression in the LFB and commissures.

(M) Retrogradely labeled soma in the midbrain, in both tectum and tegmentum, approx. 4 mm away from the injection site. For *Pleurodeles*, scale bars in overview images and magnifications represent 200 and 100 μm. For additional examples (n = 4 total), see Figure S6.

Abbreviations: ant. com., anterior commissure; APOA, anterior preoptic area; CeA, central amygdala; cont, contralateral; hip. com, hippocampal commissure; ipsi, ipsilateral; LA, lateral amygdala; LFB, lateral forebrain bundle; Sept, septum; Str, striatal neuropil; Tec, tectum; see also Figures 1, 2, 3, 4, 5, and 6.

Please cite this article in press as: Jaeger et al., Adeno-associated viral tools to trace neural development and connectivity across amphibians, Developmental Cell (2024), https://doi.org/10.1016/j.devcel.2024.10.025

on species-specific[115] and even cell-type-specific differences of intracellular processing of viral particles.

Capturing isochronic cohorts of neurons by developmental time using AAVs

In invertebrate and vertebrate nervous systems, the position, connectivity, and functional properties of a neuron are often correlated with its developmental history.[40,116–120] Our study demonstrates that intraventricular injection of AAVs in the brain and spinal cord of developing amphibians reliably transduces neuronal populations that develop around the time of injection, termed isochronic cohorts. This ability to label and target isochronic cohorts will inform long-standing questions in developmental neurobiology, including whether and how neural circuits are remodeled during metamorphosis[121–123] and after injury.

Comparing isochronic cohorts of neurons across species will also shed light on the evolution of regional subdivisions and neural circuits of the CNS. As in mammals, the amphibian pallium, optic tectum, and spinal cord develop by adding new neuronal layers, wedges, and domains in precise temporal patterns. Labeling and manipulating these cohorts can clarify relationships between neuronal birthdate and connectivity and enable testing the hypothesis that neurons that are born together wire together.[117] In an evolutionary framework, this may reveal general principles for the assembly of central neural circuits.

Tracing and manipulation of neural circuits using AAVs

The conserved ability of AAVrg to travel in a retrograde manner in both *Xenopus* and *Pleurodeles* has significant potential for the characterization and manipulation of amphibian neural circuits—critical to establish a complete picture of vertebrate brain evolution and to reveal adaptations for life on land.

Our data begin to demonstrate how the improved quality, scale, and resolution of AAV-based tracing data will empower anatomical comparisons across species. AAVrg-based tracing in *Xenopus* confirms the pallial connections reported in a distantly related frog species.[94,95] The direct projections from the midbrain tectum and tegmentum to the dorsal pallium that we observe in *Pleurodeles* resemble projections documented in other vertebrates. For example, projections from the torus semicircularis to the pallium in zebrafish are implicated in processing lateral line inputs,[124,125] while dopaminergic projections from the tegmentum to the pallium (resembling the ventral tegmental-cortical projections in mammals) have been identified in the toad *Bombina orientalis*.[96,126] Further investigation of analogous direct projections in salamanders will yield insights into the evolution of midbrain-pallial connectivity in vertebrates.

AAV-based tracing experiments not only yield data with a high signal-to-noise ratio but are also compatible with whole-brain clearing and gene expression profiling[127,128] and can be further tailored to specific neuron types with cell-type-specific promoters or enhancers.[38,99] The integration of these tools will produce multimodal, high-resolution atlases for the amphibian brain, complementing those available for fish and mammals.[127,129–132] In addition, an application of particular interest to neuroscientists is to express optogenetic actuators in specific populations of cells defined by their projection identities. Given the transparency of *Xenopus* and *Pleurodeles* at early developmental stages and the existence of non-pigmented strains, the use of light to non-invasively stimulate or inhibit subpopulations of neurons and probe their role in behavior is now feasible.

The initial AAV toolkit we have established thus opens avenues for developmental, anatomical, functional, and evolutionary studies of the amphibian CNS.

Limitations of the study

This study was carried out across three species and multiple research groups. These species exhibit differences in their anatomical and physiological characteristics—including husbandry conditions, animal size, cell size, brain ventricle volume, and progenitor properties—that challenge the standardization of experimental protocols across species and laboratories. Our experiments were thus not designed for direct quantitative comparisons of transduction efficiencies between species but rather tailored to identify the best-performing AAVs per species.

We note that expression levels in *P. bedriagae* were very low for tadpoles and absent in adults. This low success rate may stem from high genetic variability, or variation in immune status of these wild-caught animals, expression rates below the detection limit, or *Pelophylax*-specific AAV biology. Low animal availability limited our ability to perform the same number of experiments as in the other two species, resulting in reduced sample size and screening coverage.

Our investigation of the mechanisms underlying the labeling of temporal cohorts of neurons in developing larvae was limited to the best serotype-promoter combination for each species—AAV5-CAG in *Xenopus* and AAV-PHP.eB-CAG in *Pleurodeles*. Mechanisms of viral uptake may depend on the capsid protein sequence or the species itself and thus cannot be generalized to other serotypes.

RESOURCE AVAILABILITY

Lead contact

Further information and requests for resources and reagents should be directed to and will be fulfilled by the lead contact, Lora B. Sweeney (lora.sweeney@ist.ac.at).

Materials availability

This study did not generate new unique reagents.

Data and code availability

FAMD RStudio code and raw data used for analysis of post-metamorphic *P. waltl* injection outcomes are available via Dryad repository: https://doi.org/10.5061/dryad.mpg4f4r89. Any additional information required to reanalyze the data reported in this paper is available from the lead contact upon request.

ACKNOWLEDGMENTS

We thank members of the Sweeney, Tosches, Shein-Idelson, Yamaguchi, Kelley, and Cline Labs for their contributions to this project, discussion, and support. We additionally thank the Beckman Institute CLOVER Center and Viviana Gradinaru (Caltech), Kimberly Ritola (UNC NeuroTools), and Flavia Gomez-Leite (ISTA Viral Core) for AAV production and consultation; Andras Simon and Alberto Joven (Karolinska Institute) for feedback; Elizabeth Bagnato-Cohen (Columbia) for project coordination; our animal care and imaging facilities; the amphibian stock centers (NXR, EXRC, and XenopusExpress); and our funding sources: NSF IOS 2110086 (D.B.K., L.B.S., M.A.T., A.Y., and H.T.C.); US-Israel Binational Science Foundation (BSF) 2020702 (M.S.-I.); FTI Strategy Lower Austria Dissertation FT121-D-046 (D.V.); Horizon Europe ERC Starting Grant 101041551 and Special Research Programme (SFB) of the Austrian

Science Fund (FWF) project F7814-B (L.B.S.); NIH grant R35GM146973, Rita Allen Foundation Award GA_032522_FE, and CZI Ben Barres Early Career Acceleration Award 2023-331758 (M.A.T.); EMBO Long-Term Fellowship ALTF 874-2021 (A.D.); and NSF GRFP DGE 2036197 (E.C.B.J.).

AUTHOR CONTRIBUTIONS

M.A.T. and L.B.S. led and coordinated the project. E.C.B.J., D.V., A.D., H.T.C., T.F.S., D.B.K., A.Y., M.S.-I., M.A.T., and L.B.S. devised the project and implemented experiments. E.C.B.J., A.D., J.W., A.O.G., and M.A.T. collected the *Pleurodeles* data. D.V., A.L.N., G.I., R.C.A., F.B., F.A.T., A.Y., and L.B.S. collected the *Xenopus* data. N.Z., A.S., and M.S.-I. collected the *Pelophylax* data. E.C.B.J., D.V., A.D., N.Z., G.I., M.A.T., and L.B.S. analyzed the data. E.C.B.J., D.V., A.D., M.A.T., and L.B.S. wrote the manuscript. H.T.C., T.F.S., D.B.K., A.Y., and M.S.-I. edited the manuscript and provided critical feedback on the project.

DECLARATION OF INTERESTS

The authors declare no competing interests.

STAR★METHODS

Detailed methods are provided in the online version of this paper and include the following:

- KEY RESOURCES TABLE
- EXPERIMENTAL MODEL AND STUDY PARTICIPANT DETAILS
- METHOD DETAILS
  - Intracerebroventricular, intraspinoventricular, and intraparenchymal injection in Xenopus tadpoles
  - Intracerebroventricular injection in Pleurodeles larvae
  - Intracerebroventricular injection in Pelophylax bedriagae tadpoles
  - Intrapallial injections in Xenopus juveniles and adults
  - Intrapallial injections in post-metamorphic Pleurodeles
  - EdU injections in *Xenopus* tadpoles
  - EdU injections in *Pleurodeles* larvae
  - Staining protocols
  - Analysis of variable injection outcomes in post-metamorphic Pleurodeles using factor analysis for mixed data (FAMD)
- QUANTIFICATION AND STATISTICAL ANALYSIS

SUPPLEMENTAL INFORMATION

Supplemental information can be found online at https://doi.org/10.1016/j.devcel.2024.10.025.

Received: April 13, 2024
Revised: September 19, 2024
Accepted: October 30, 2024
Published: November 26, 2024

REFERENCES

1. Hamburger, V. (1984). Hilde Mangold, co-discoverer of the organizer. J. Hist. Biol. *17*, 1–11. https://doi.org/10.1007/BF00397500.
2. Del Castillo, J., and Katz, B. (1954). Quantal components of the end plate potential. J. Physiol. *124*, 560–573. https://doi.org/10.1113/jphysiol.1954.sp005129.
3. Tazaki, A., Tanaka, E.M., and Fei, J.-F. (2017). Salamander spinal cord regeneration: the ultimate positive control in vertebrate spinal cord regeneration. Dev. Biol. *432*, 63–71. https://doi.org/10.1016/j.ydbio.2017.09.034.
4. Kwong-Brown, U., Tobias, M.L., Elias, D.O., Hall, I.C., Elemans, C.P., and Kelley, D.B. (2019). The return to water in ancestral Xenopus was accompanied by a novel mechanism for producing and shaping vocal signals. eLife *8*, e39946. https://doi.org/10.7554/eLife.39946.
5. Kelley, D.B., Ballagh, I.H., Barkan, C.L., Bendesky, A., Elliott, T.M., Evans, B.J., Hall, I.C., Kwon, Y.M., Kwong-Brown, U., Leininger, E.C., et al. (2020). Generation, coordination, and evolution of neural circuits for vocal communication. J. Neurosci. *40*, 22–36. https://doi.org/10.1523/JNEUROSCI.0736-19.2019.
6. Iyer, A.A., and Briggman, K.L. (2021). Amphibian behavioral diversity offers insights into evolutionary neurobiology. Curr. Opin. Neurobiol. *71*, 19–28. https://doi.org/10.1016/j.conb.2021.07.015.
7. Wei, X., Fu, S., Li, H., Liu, Y., Wang, S., Feng, W., Yang, Y., Liu, X., Zeng, Y.-Y., Cheng, M., et al. (2022). Single-cell Stereo-seq reveals induced progenitor cells involved in axolotl brain regeneration. Science *377*, eabp9444. https://doi.org/10.1126/science.abp9444.
8. Lust, K., Maynard, A., Gomes, T., Fleck, J.S., Camp, J.G., Tanaka, E.M., and Treutlein, B. (2022). Single-cell analyses of axolotl telencephalon organization, neurogenesis, and regeneration. Science *377*, eabp9262. https://doi.org/10.1126/science.abp9262.
9. Flaive, A., and Ryczko, D. (2022). From retina to motoneurons: A substrate for visuomotor transformation in salamanders. J. Comp. Neurol. *530*, 2518–2536. https://doi.org/10.1002/cne.25348.
10. Offner, T., Weiss, L., Daume, D., Berk, A., Inderthal, T.J., Manzini, I., and Hassenklöver, T. (2023). Functional odor map heterogeneity is based on multifaceted glomerular connectivity in larval Xenopus olfactory bulb. iScience *26*, 107518. https://doi.org/10.1016/j.isci.2023.107518.
11. He, H.-Y., Ahsan, A., Bera, R., McLain, N., Faulkner, R., Ramachandran, K.V., Margolis, S.S., and Cline, H.T. (2023). Neuronal membrane proteasomes regulate neuronal circuit activity in vivo and are required for learning-induced behavioral plasticity. Proc. Natl. Acad. Sci. USA *120*, e2216537120. https://doi.org/10.1073/pnas.2216537120.
12. Joven, A., Wang, H., Pinheiro, T., Hameed, L.S., Belnoue, L., and Simon, A. (2018). Cellular basis of brain maturation and acquisition of complex behaviors in salamanders. Development *145*, dev160051. https://doi.org/10.1242/dev.160051.
13. Kakebeen, A.D., Chitsazan, A.D., Williams, M.C., Saunders, L.M., and Wills, A.E. (2020). Chromatin accessibility dynamics and single cell RNA-Seq reveal new regulators of regeneration in neural progenitors. eLife *9*, e52648. https://doi.org/10.7554/eLife.52648.
14. Willsey, H.R., Exner, C.R.T., Xu, Y., Everitt, A., Sun, N., Wang, B., Dea, J., Schmunk, G., Zaltsman, Y., Teerikorpi, N., et al. (2021). Parallel in vivo analysis of large-effect autism genes implicates cortical neurogenesis and estrogen in risk and resilience. Neuron *109*, 788–804.e8. https://doi.org/10.1016/j.neuron.2021.01.002.
15. Exner, C.R.T., and Willsey, H.R. (2021). Xenopus leads the way: frogs as a pioneering model to understand the human brain. Genesis *59*, e23405. https://doi.org/10.1002/dvg.23405.
16. MacIver, M.A., and Finlay, B.L. (2022). The neuroecology of the water-to-land transition and the evolution of the vertebrate brain. Philos. Trans. R. Soc. Lond. B Biol. Sci. *377*, 20200523. https://doi.org/10.1098/rstb.2020.0523.
17. Striedter, G.F., and Northcutt, R.G. (2019). Brains through Time: A Natural History of Vertebrates (Oxford University Press). https://doi.org/10.1093/oso/9780195125689.001.0001.
18. Woych, J., Ortega Gurrola, A., Deryckere, A., Jaeger, E.C.B., Gumnit, E., Merello, G., Gu, J., Joven Araus, A., Leigh, N.D., Yun, M., et al. (2022). Cell-type profiling in salamanders identifies innovations in vertebrate forebrain evolution. Science *377*, eabp9186. https://doi.org/10.1126/science.abp9186.
19. Joven, A., Kirkham, M., and Simon, A. (2015). Husbandry of Spanish ribbed newts (Pleurodeles waltl). Methods Mol. Biol. *1290*, 47–70. https://doi.org/10.1007/978-1-4939-2495-0_4.
20. Zhang, L., and Lu, X. (2013). Sexual size dimorphism in anurans: ontogenetic determination revealed by an across-species comparison. Evol. Biol. *40*, 84–91. https://doi.org/10.1007/s11692-012-9187-2.
21. Khattak, S., Murawala, P., Andreas, H., Kappert, V., Schuez, M., Sandoval-Guzmán, T., Crawford, K., and Tanaka, E.M. (2014).

Optimized axolotl (Ambystoma mexicanum) husbandry, breeding, metamorphosis, transgenesis and tamoxifen-mediated recombination. Nat. Protoc. *9*, 529–540. https://doi.org/10.1038/nprot.2014.040.

22. Haas, K., Jensen, K., Sin, W.C., Foa, L., and Cline, H.T. (2002). Targeted electroporation in Xenopus tadpoles in vivo–from single cells to the entire brain. Differentiation *70*, 148–154. https://doi.org/10.1046/j.1432-0436.2002.700404.x.

23. Edwards-Faret, G., de Vin, F., Slezak, M., Gollenbeck, L., Karaman, R., Shinmyo, Y., Batiuk, M.Y., Pando, C.M., Urschitz, J., Rincon, M.Y., et al. (2023). A new technical approach for cross-species examination of neuronal wiring and adult neuron-glia functions. Neuroscience *508*, 40–51. https://doi.org/10.1016/j.neuroscience.2022.11.029.

24. Montreau, N., Vaur, S., Dautry, F., and Andéol, Y. (2003). Injection of exogenous RNA in amphibian oocytes leads to RNA level fluctuations which are sensitive to cordycepin, an RNA chain elongation terminator. C. R. Biol. *326*, 1135–1147. https://doi.org/10.1016/j.crvi.2003.10.002.

25. Haggerty, D.L., Grecco, G.G., Reeves, K.C., and Atwood, B. (2020). Adeno-associated viral vectors in neuroscience research. Mol. Ther. Methods Clin. Dev. *17*, 69–82. https://doi.org/10.1016/j.omtm.2019.11.012.

26. Nassi, J.J., Cepko, C.L., Born, R.T., and Beier, K.T. (2015). Neuroanatomy goes viral! Front. Neuroanat. *9*, 80. https://doi.org/10.3389/fnana.2015.00080.

27. Challis, R.C., Ravindra Kumar, S., Chen, X., Goertsen, D., Coughlin, G.M., Hori, A.M., Chuapoco, M.R., Otis, T.S., Miles, T.F., and Gradinaru, V. (2022). Adeno-associated virus toolkit to target diverse brain cells. Annu. Rev. Neurosci. *45*, 447–469. https://doi.org/10.1146/annurev-neuro-111020-100834.

28. Riyad, J.M., and Weber, T. (2021). Intracellular trafficking of adeno-associated virus (AAV) vectors: challenges and future directions. Gene Ther. *28*, 683–696. https://doi.org/10.1038/s41434-021-00243-z.

29. Bedbrook, C.N., Deverman, B.E., and Gradinaru, V. (2018). Viral strategies for targeting the central and peripheral nervous systems. Annu. Rev. Neurosci. *41*, 323–348. https://doi.org/10.1146/annurev-neuro-080317-062048.

30. Rajasethupathy, P., Ferenczi, E., and Deisseroth, K. (2016). Targeting neural circuits. Cell *165*, 524–534. https://doi.org/10.1016/j.cell.2016.03.047.

31. Hocquemiller, M., Giersch, L., Audrain, M., Parker, S., and Cartier, N. (2016). Adeno-associated virus-based gene therapy for CNS diseases. Hum. Gene Ther. *27*, 478–496. https://doi.org/10.1089/hum.2016.087.

32. Choudhury, S.R., Hudry, E., Maguire, C.A., Sena-Esteves, M., Breakefield, X.O., and Grandi, P. (2017). Viral vectors for therapy of neurologic diseases. Neuropharmacology *120*, 63–80. https://doi.org/10.1016/j.neuropharm.2016.02.013.

33. McCown, T.J., Xiao, X., Li, J., Breese, G.R., and Samulski, R.J. (1996). Differential and persistent expression patterns of CNS gene transfer by an adeno-associated virus (AAV) vector. Brain Res. *713*, 99–107. https://doi.org/10.1016/0006-8993(95)01488-8.

34. Jang, M.J., Coughlin, G.M., Jackson, C.R., Chen, X., Chuapoco, M.R., Vendemiatti, J.L., Wang, A.Z., and Gradinaru, V. (2023). Spatial transcriptomics for profiling the tropism of viral vectors in tissues. Nat. Biotechnol. *41*, 1272–1286. https://doi.org/10.1038/s41587-022-01648-w.

35. Lopez-Gordo, E., Chamberlain, K., Riyad, J.M., Kohlbrenner, E., and Weber, T. (2024). Natural adeno-associated virus serotypes and engineered adeno-associated virus capsid variants: tropism differences and mechanistic insights. Viruses *16*, 442. https://doi.org/10.3390/v16030442.

36. Ben-Simon, Y., Hooper, M., Narayan, S., Daigle, T., Dwivedi, D., Way, S.W., Oster, A., Stafford, D.A., Mich, J.K., Taormina, M.J., et al. (2024). A suite of enhancer AAVs and transgenic mouse lines for genetic access to cortical cell types. Preprint at bioRxiv. https://doi.org/10.1101/2024.06.10.597244.

37. Mich, J.K., Graybuck, L.T., Hess, E.E., Mahoney, J.T., Kojima, Y., Ding, Y., Somasundaram, S., Miller, J.A., Kalmbach, B.E., Radaelli, C., et al. (2021). Functional enhancer elements drive subclass-selective expression from mouse to primate neocortex. Cell Rep. *34*, 108754. https://doi.org/10.1016/j.celrep.2021.108754.

38. Dimidschstein, J., Chen, Q., Tremblay, R., Rogers, S.L., Saldi, G.-A., Guo, L., Xu, Q., Liu, R., Lu, C., Chu, J., et al. (2016). A viral strategy for targeting and manipulating interneurons across vertebrate species. Nat. Neurosci. *19*, 1743–1749. https://doi.org/10.1038/nn.4430.

39. Chakrabarty, P., Rosario, A., Cruz, P., Siemienski, Z., Ceballos-Diaz, C., Crosby, K., Jansen, K., Borchelt, D.R., Kim, J.-Y., Jankowsky, J.L., et al. (2013). Capsid serotype and timing of injection determines AAV transduction in the neonatal mice brain. PLoS One *8*, e67680. https://doi.org/10.1371/journal.pone.0067680.

40. Donato, F., Jacobsen, R.I., Moser, M.-B., and Moser, E.I. (2017). Stellate cells drive maturation of the entorhinal-hippocampal circuit. Science *355*, eaai8178. https://doi.org/10.1126/science.aai8178.

41. Card, J.P., Rinaman, L., Lynn, R.B., Lee, B.H., Meade, R.P., Miselis, R.R., and Enquist, L.W. (1993). Pseudorabies virus infection of the rat central nervous system: ultrastructural characterization of viral replication, transport, and pathogenesis. J. Neurosci. *13*, 2515–2539. https://doi.org/10.1523/JNEUROSCI.13-06-02515.1993.

42. Faulkner, R.L., Wall, N.R., Callaway, E.M., and Cline, H.T. (2021). Application of recombinant rabies virus to Xenopus tadpole brain. eNeuro *8*, ENEURO.0477-20.2021. https://doi.org/10.1523/ENEURO.0477-20.2021.

43. Wu, G.Y., Zou, D.J., Koothan, T., and Cline, H.T. (1995). Infection of frog neurons with vaccinia virus permits in vivo expression of foreign proteins. Neuron *14*, 681–684. https://doi.org/10.1016/0896-6273(95)90211-2.

44. Yamaguchi, A., Woller, D.J., and Rodrigues, P. (2018). Development of an acute method to deliver transgenes into the brains of adult Xenopus laevis. Front. Neural Circuits *12*, 92. https://doi.org/10.3389/fncir.2018.00092.

45. Dutton, J.R., Daughters, R.S., Chen, Y., O'Neill, K.E., and Slack, J.M.W. (2009). Use of adenovirus for ectopic gene expression in Xenopus. Dev. Dyn. *238*, 1412–1421. https://doi.org/10.1002/dvdy.21932.

46. Khattak, S., Sandoval-Guzmán, T., Stanke, N., Protze, S., Tanaka, E.M., and Lindemann, D. (2013). Foamy virus for efficient gene transfer in regeneration studies. BMC Dev. Biol. *13*, 17. https://doi.org/10.1186/1471-213X-13-17.

47. Whited, J.L., Tsai, S.L., Beier, K.T., White, J.N., Piekarski, N., Hanken, J., Cepko, C.L., and Tabin, C.J. (2013). Pseudotyped retroviruses for infecting axolotl in vivo and in vitro. Development *140*, 1137–1146. https://doi.org/10.1242/dev.087734.

48. Oliveira, C.R., Lemaitre, R., Murawala, P., Tazaki, A., Drechsel, D.N., and Tanaka, E.M. (2018). Pseudotyped baculovirus is an effective gene expression tool for studying molecular function during axolotl limb regeneration. Dev. Biol. *433*, 262–275. https://doi.org/10.1016/j.ydbio.2017.10.008.

49. San Mauro, D., Vences, M., Alcobendas, M., Zardoya, R., and Meyer, A. (2005). Initial diversification of living amphibians predated the breakup of Pangaea. Am. Nat. *165*, 590–599. https://doi.org/10.1086/429523.

50. Feng, Y.-J., Blackburn, D.C., Liang, D., Hillis, D.M., Wake, D.B., Cannatella, D.C., and Zhang, P. (2017). Phylogenomics reveals rapid, simultaneous diversification of three major clades of Gondwanan frogs at the Cretaceous-Paleogene boundary. Proc. Natl. Acad. Sci. USA *114*, E5864–E5870. https://doi.org/10.1073/pnas.1704632114.

51. Passini, M.A., and Wolfe, J.H. (2001). Widespread gene delivery and structure-specific patterns of expression in the brain after intraventricular injections of neonatal mice with an adeno-associated virus vector. J. Virol. *75*, 12382–12392. https://doi.org/10.1128/JVI.75.24.12382-12392.2001.

52. Passini, M.A., Watson, D.J., Vite, C.H., Landsburg, D.J., Feigenbaum, A.L., and Wolfe, J.H. (2003). Intraventricular brain injection of adeno-associated virus type 1 (AAV1) in neonatal mice results in complementary patterns of

neuronal transduction to AAV2 and total long-term correction of storage lesions in the brains of beta-glucuronidase-deficient mice. J. Virol. *77*, 7034–7040. https://doi.org/10.1128/jvi.77.12.7034-7040.2003.

53. Thuret, R., Auger, H., and Papalopulu, N. (2015). Analysis of neural progenitors from embryogenesis to juvenile adult in Xenopus laevis reveals biphasic neurogenesis and continuous lengthening of the cell cycle. Biol. Open *4*, 1772–1781. https://doi.org/10.1242/bio.013391.
54. Mogi, K., Adachi, T., Izumi, S., and Toyoizumi, R. (2012). Visualisation of cerebrospinal fluid flow patterns in albino Xenopus larvae in vivo. Fluids Barriers CNS *9*, 9. https://doi.org/10.1186/2045-8118-9-9.
55. Vandenberghe, L.H., Breous, E., Nam, H.J., Gao, G., Xiao, R., Sandhu, A., Johnston, J., Debyser, Z., Agbandje-McKenna, M., and Wilson, J.M. (2009). Naturally occurring singleton residues in AAV capsid impact vector performance and illustrate structural constraints. Gene Ther. *16*, 1416–1428. https://doi.org/10.1038/gt.2009.101.
56. Gallien, L., and Durocher, M. (1957). Table chronologique du développement chez *Pleurodeles waltlII* Michah. Bull. Biol. *2*, 1–19.
57. Kügler, S., Kilic, E., and Bähr, M. (2003). Human synapsin 1 gene promoter confers highly neuron-specific long-term transgene expression from an adenoviral vector in the adult rat brain depending on the transduced area. Gene Ther. *10*, 337–347. https://doi.org/10.1038/sj.gt.3301905.
58. Niwa, H., Yamamura, K., and Miyazaki, J. (1991). Efficient selection for high-expression transfectants with a novel eukaryotic vector. Gene *108*, 193–199. https://doi.org/10.1016/0378-1119(91)90434-D.
59. P.D. Nieuwkoop, and J. Faber, eds. (1994). Normal Table of Xenopus laevis (Daudin): A Systematical and Chronological Survey of the Development from the Fertilized Egg Till the End of Metamorphosis, 2nd edn (Garland Publishing).
60. Bandín, S., Morona, R., Moreno, N., and González, A. (2013). Regional expression of Pax7 in the brain of Xenopus laevis during embryonic and larval development. Front. Neuroanat. *7*, 48. https://doi.org/10.3389/fnana.2013.00048.
61. Ruiz, V.L., and Robert, J. (2023). The amphibian immune system. Philos. Trans. R. Soc. Lond. B Biol. Sci. *378*, 20220123. https://doi.org/10.1098/rstb.2022.0123.
62. Moreno, N., Bachy, I., Rétaux, S., and González, A. (2004). LIM-homeodomain genes as developmental and adult genetic markers of Xenopus forebrain functional subdivisions. J. Comp. Neurol. *472*, 52–72. https://doi.org/10.1002/cne.20046.
63. Good, P.J. (1995). A conserved family of elav-like genes in vertebrates. Proc. Natl. Acad. Sci. USA *92*, 4557–4561. https://doi.org/10.1073/pnas.92.10.4557.
64. Perron, M., Furrer, M.P., Wegnez, M., and Théodore, L. (1999). Xenopus elav-like genes are differentially expressed during neurogenesis. Mech. Dev. *84*, 139–142. https://doi.org/10.1016/s0925-4773(99)00056-8.
65. Gosner, K. (1960). A simplified table for staging anuran embryos and larvae with notes on identification. Herpetologica *6*, 183–190.
66. Pesarakloo, A. (2019). Life history of the Levant water frog, Pelophylax bedriagae (Amphibia: Anura: Ranidae) in western Iran. JAD *1*, 11–19. https://doi.org/10.29252/JAD.2019.1.1.2.
67. Wullimann, M.F., Rink, E., Vernier, P., and Schlosser, G. (2005). Secondary neurogenesis in the brain of the African clawed frog, Xenopus laevis, as revealed by PCNA, Delta-1, Neurogenin-related-1, and NeuroD expression. J. Comp. Neurol. *489*, 387–402. https://doi.org/10.1002/cne.20634.
68. Moreno, N., and González, A. (2017). Pattern of neurogenesis and identification of neuronal progenitor subtypes during pallial development in Xenopus laevis. Front. Neuroanat. *11*, 24. https://doi.org/10.3389/fnana.2017.00024.
69. Zeng, C., Pan, F., Jones, L.A., Lim, M.M., Griffin, E.A., Sheline, Y.I., Mintun, M.A., Holtzman, D.M., and Mach, R.H. (2010). Evaluation of 5-ethynyl-2′-deoxyuridine staining as a sensitive and reliable method for studying cell proliferation in the adult nervous system. Brain Res. *1319*, 21–32. https://doi.org/10.1016/j.brainres.2009.12.092.
70. Salic, A., and Mitchison, T.J. (2008). A chemical method for fast and sensitive detection of DNA synthesis in vivo. Proc. Natl. Acad. Sci. USA *105*, 2415–2420. https://doi.org/10.1073/pnas.0712168105.
71. Prestige, M.C. (1973). Gradients in time of origin of tadpoles motorneurons. Brain Res. *59*, 400–404. https://doi.org/10.1016/0006-8993(73)90280-1.
72. Gao, J., Lu, Y., Luo, Y., Duan, X., Chen, P., Zhang, X., Wu, X., Qiu, M., and Shen, W. (2023). β-catenin and SOX2 Interaction Regulate Visual Experience-Dependent Cell Homeostasis in the Developing Xenopus thalamus. Int. J. Mol. Sci. *24*, 13593. https://doi.org/10.3390/ijms241713593.
73. Bandín, S., Morona, R., and González, A. (2015). Prepatterning and patterning of the thalamus along embryonic development of Xenopus laevis. Front. Neuroanat. *9*, 107. https://doi.org/10.3389/fnana.2015.00107.
74. Bernardini, S., Gargioli, C., Cannata, S.M., and Filoni, S. (2010). Neurogenesis during optic tectum regeneration in Xenopus laevis. Dev. Growth Differ. *52*, 365–376. https://doi.org/10.1111/j.1440-169X.2010.01176.x.
75. Straznicky, K., and Gaze, R.M. (1972). The development of the tectum in *Xenopus laevis*: an autoradiographic study. J. Embryol. Exp. Morphol. *28*, 87–115. https://doi.org/10.1242/dev.28.1.87.
76. Zhou, K., Han, J., Wang, Y., Zhang, Y., and Zhu, C. (2022). Routes of administration for adeno-associated viruses carrying gene therapies for brain diseases. Front. Mol. Neurosci. *15*, 988914. https://doi.org/10.3389/fnmol.2022.988914.
77. Gao, J., Ruan, H., Qi, X., Tao, Y., Guo, X., and Shen, W. (2016). HDAC3 but not HDAC2 mediates visual experience-dependent radial glia proliferation in the developing Xenopus tectum. Front. Cell. Neurosci. *10*, 221. https://doi.org/10.3389/fncel.2016.00221.
78. Muñoz, R., Edwards-Faret, G., Moreno, M., Zuñiga, N., Cline, H., and Larraín, J. (2015). Regeneration of Xenopus laevis spinal cord requires Sox2/3 expressing cells. Dev. Biol. *408*, 229–243. https://doi.org/10.1016/j.ydbio.2015.03.009.
79. Choi, H.M.T., Schwarzkopf, M., Fornace, M.E., Acharya, A., Artavanis, G., Stegmaier, J., Cunha, A., and Pierce, N.A. (2018). Third-generation in situ hybridization chain reaction: multiplexed, quantitative, sensitive, versatile, robust. Development *145*, dev165753. https://doi.org/10.1242/dev.165753.
80. Schwerk, C., Tenenbaum, T., Kim, K.S., and Schroten, H. (2015). The choroid plexus-a multi-role player during infectious diseases of the CNS. Front. Cell. Neurosci. *9*, 80. https://doi.org/10.3389/fncel.2015.00080.
81. Mullen, R.J., Buck, C.R., and Smith, A.M. (1992). NeuN, a neuronal specific nuclear protein in vertebrates. Development *116*, 201–211. https://doi.org/10.1242/dev.116.1.201.
82. Gittins, R., and Harrison, P.J. (2004). Neuronal density, size and shape in the human anterior cingulate cortex: a comparison of Nissl and NeuN staining. Brain Res. Bull. *63*, 155–160. https://doi.org/10.1016/j.brainresbull.2004.02.005.
83. Takamori, S., Rhee, J.S., Rosenmund, C., and Jahn, R. (2000). Identification of a vesicular glutamate transporter that defines a glutamatergic phenotype in neurons. Nature *407*, 189–194. https://doi.org/10.1038/35025070.
84. Gonzalez-Sandoval, A., Pekrun, K., Tsuji, S., Zhang, F., Hung, K.L., Chang, H.Y., and Kay, M.A. (2023). The AAV capsid can influence the epigenetic marking of rAAV delivered episomal genomes in a species dependent manner. Nat. Commun. *14*, 2448. https://doi.org/10.1038/s41467-023-38106-3.
85. Fei, J.-F., Schuez, M., Tazaki, A., Taniguchi, Y., Roensch, K., and Tanaka, E.M. (2014). CRISPR-mediated genomic deletion of Sox2 in the axolotl shows a requirement in spinal cord neural stem cell amplification during

tail regeneration. Stem Cell Rep. *3*, 444–459. https://doi.org/10.1016/j.stemcr.2014.06.018.

86. Cura Costa, E., Otsuki, L., Rodrigo Albors, A., Tanaka, E.M., and Chara, O. (2021). Spatiotemporal control of cell cycle acceleration during axolotl spinal cord regeneration. eLife *10*, e55665. https://doi.org/10.7554/eLife.55665.
87. Kirkham, M., Hameed, L.S., Berg, D.A., Wang, H., and Simon, A. (2014). Progenitor cell dynamics in the Newt telencephalon during homeostasis and neuronal regeneration. Stem Cell Rep. *2*, 507–519. https://doi.org/10.1016/j.stemcr.2014.01.018.
88. Das, A., Vijayan, M., Walton, E.M., Stafford, V.G., Fiflis, D.N., and Asokan, A. (2022). Epigenetic silencing of recombinant adeno-associated virus genomes by NP220 and the HUSH complex. J. Virol. *96*, e0203921. https://doi.org/10.1128/JVI.02039-21.
89. Tobias, M.L., Marin, M.L., and Kelley, D.B. (1991). Development of functional sex differences in the larynx of Xenopus laevis. Dev. Biol. *147*, 251–259. https://doi.org/10.1016/s0012-1606(05)80022-3.
90. Herrick, C.J. (1948). The Brain of the Tiger Salamander, Ambystoma tigrinum (University of Chicago Press). https://doi.org/10.5962/bhl.title.6375.
91. Lê, S., Josse, J., and Husson, F. (2008). FactoMineR: an *R* package for multivariate analysis. J. Stat. Softw. *25*, 1–18. https://doi.org/10.18637/jss.v025.i01.
92. Kim, J.-Y., Grunke, S.D., Levites, Y., Golde, T.E., and Jankowsky, J.L. (2014). Intracerebroventricular viral injection of the neonatal mouse brain for persistent and widespread neuronal transduction. J. Vis. Exp. 51863. https://doi.org/10.3791/51863.
93. Tervo, D.G.R., Hwang, B.-Y., Viswanathan, S., Gaj, T., Lavzin, M., Ritola, K.D., Lindo, S., Michael, S., Kuleshova, E., Ojala, D., et al. (2016). A designer AAV variant permits efficient retrograde access to projection neurons. Neuron *92*, 372–382. https://doi.org/10.1016/j.neuron.2016.09.021.
94. Westhoff, G., and Roth, G. (2002). Morphology and projection pattern of medial and dorsal pallial neurons in the frog Discoglossus pictus and the salamander Plethodon jordani. J. Comp. Neurol. *445*, 97–121. https://doi.org/10.1002/cne.10136.
95. Roth, G., Laberge, F., Mühlenbrock-Lenter, S., and Grunwald, W. (2007). Organization of the pallium in the fire-bellied toad Bombina orientalis. I: Morphology and axonal projection pattern of neurons revealed by intracellular biocytin labeling. J. Comp. Neurol. *501*, 443–464. https://doi.org/10.1002/cne.21255.
96. Freudenmacher, L., Schauer, M., Walkowiak, W., and von Twickel, A. (2020). Refinement of the dopaminergic system of anuran amphibians based on connectivity with habenula, basal ganglia, limbic system, pallium, and spinal cord. J. Comp. Neurol. *528*, 972–988. https://doi.org/10.1002/cne.24793.
97. Chen, X., Wolfe, D.A., Bindu, D.S., Zhang, M., Taskin, N., Goertsen, D., Shay, T.F., Sullivan, E.E., Huang, S.-F., Ravindra Kumar, S., et al. (2023). Functional gene delivery to and across brain vasculature of systemic AAVs with endothelial-specific tropism in rodents and broad tropism in primates. Nat. Commun. *14*, 3345. https://doi.org/10.1038/s41467-023-38582-7.
98. Chen, X., Ravindra Kumar, S., Adams, C.D., Yang, D., Wang, T., Wolfe, D.A., Arokiaraj, C.M., Ngo, V., Campos, L.J., Griffiths, J.A., et al. (2022). Engineered AAVs for non-invasive gene delivery to rodent and non-human primate nervous systems. Neuron *110*, 2242–2257.e6. https://doi.org/10.1016/j.neuron.2022.05.003.
99. Spool, J.A., Macedo-Lima, M., Scarpa, G., Morohashi, Y., Yazaki-Sugiyama, Y., and Remage-Healey, L. (2021). Genetically identified neurons in avian auditory pallium mirror core principles of their mammalian counterparts. Curr. Biol. *31*, 2831–2843.e6. https://doi.org/10.1016/j.cub.2021.04.039.
100. Düring, D.N., Dittrich, F., Rocha, M.D., Tachibana, R.O., Mori, C., Okanoya, K., Boehringer, R., Ehret, B., Grewe, B.F., Gerber, S., et al. (2020). Fast retrograde access to projection neuron circuits underlying vocal learning in songbirds. Cell Rep. *33*, 108364. https://doi.org/10.1016/j.celrep.2020.108364.
101. Heston, J.B., and White, S.A. (2015). Behavior-linked FoxP2 regulation enables zebra finch vocal learning. J. Neurosci. *35*, 2885–2894. https://doi.org/10.1523/JNEUROSCI.3715-14.2015.
102. Nelson, A., Schneider, D.M., Takatoh, J., Sakurai, K., Wang, F., and Mooney, R. (2013). A circuit for motor cortical modulation of auditory cortical activity. J. Neurosci. *33*, 14342–14353. https://doi.org/10.1523/JNEUROSCI.2275-13.2013.
103. Norimoto, H., Fenk, L.A., Li, H.-H., Tosches, M.A., Gallego-Flores, T., Hain, D., Reiter, S., Kobayashi, R., Macias, A., Arends, A., et al. (2020). A claustrum in reptiles and its role in slow-wave sleep. Nature *578*, 413–418. https://doi.org/10.1038/s41586-020-1993-6.
104. Zhu, P., Narita, Y., Bundschuh, S.T., Fajardo, O., Schärer, Y.-P.Z., Chattopadhyaya, B., Bouldoires, E.A., Stepien, A.E., Deisseroth, K., Arber, S., et al. (2009). Optogenetic dissection of neuronal circuits in zebrafish using viral gene transfer and the tet system. Front. Neural Circuits *3*, 21. https://doi.org/10.3389/neuro.04.021.2009.
105. Lust, K., and Tanaka, E.M. (2024). Adeno-associated viruses for efficient gene expression in the axolotl nervous system. Preprint at bioRxiv. https://doi.org/10.1101/2024.02.15.580426.
106. Dhungel, B.P., Bailey, C.G., and Rasko, J.E.J. (2021). Journey to the center of the cell: tracing the path of AAV transduction. Trends Mol. Med. *27*, 172–184. https://doi.org/10.1016/j.molmed.2020.09.010.
107. Akache, B., Grimm, D., Pandey, K., Yant, S.R., Xu, H., and Kay, M.A. (2006). The 37/67-kilodalton laminin receptor is a receptor for adeno-associated virus serotypes 8, 2, 3, and 9. J. Virol. *80*, 9831–9836. https://doi.org/10.1128/JVI.00878-06.
108. Bantel-Schaal, U., Delius, H., Schmidt, R., and zur Hausen, H. (1999). Human adeno-associated virus type 5 is only distantly related to other known primate helper-dependent parvoviruses. J. Virol. *73*, 939–947. https://doi.org/10.1128/JVI.73.2.939-947.1999.
109. Dudek, A.M., Zabaleta, N., Zinn, E., Pillay, S., Zengel, J., Porter, C., Franceschini, J.S., Estelien, R., Carette, J.E., Zhou, G.L., et al. (2020). GPR108 is a highly conserved AAV entry factor. Mol. Ther. *28*, 367–381. https://doi.org/10.1016/j.ymthe.2019.11.005.
110. Meisen, W.H., Nejad, Z.B., Hardy, M., Zhao, H., Oliverio, O., Wang, S., Hale, C., Ollmann, M.M., and Collins, P.J. (2020). Pooled screens identify GPR108 and TM9SF2 as host cell factors critical for AAV transduction. Mol. Ther. Methods Clin. Dev. *17*, 601–611. https://doi.org/10.1016/j.omtm.2020.03.012.
111. Petrova, K., Tretiakov, M., Kotov, A., Monsoro-Burq, A.H., and Peshkin, L. (2024). A revised single-cell transcriptomic atlas of *Xenopus* embryo reveals new differentiation dynamics. Preprint at bioRxiv. https://doi.org/10.1101/2024.01.02.573882.
112. Martin, F.J., Amode, M.R., Aneja, A., Austine-Orimoloye, O., Azov, A.G., Barnes, I., Becker, A., Bennett, R., Berry, A., Bhai, J., et al. (2023). Ensembl 2023. Nucleic Acids Res. *51*, D933–D941. https://doi.org/10.1093/nar/gkac958.
113. Nevue, A.A., Sairavi, A., Huang, S.J., Nakai, H., and Mello, C.V. (2024). Genomic loss of GPR108 disrupts AAV transduction in birds. Preprint at bioRxiv. https://doi.org/10.1101/2024.05.16.589954.
114. Chan, K.Y., Jang, M.J., Yoo, B.B., Greenbaum, A., Ravi, N., Wu, W.-L., Sánchez-Guardado, L., Lois, C., Mazmanian, S.K., Deverman, B.E., et al. (2017). Engineered AAVs for efficient noninvasive gene delivery to the central and peripheral nervous systems. Nat. Neurosci. *20*, 1172–1179. https://doi.org/10.1038/nn.4593.
115. Loeb, E.J., Havlik, P.L., Elmore, Z.C., Rosales, A., Fergione, S.M., Gonzalez, T.J., Smith, T.J., Benkert, A.R., Fiflis, D.N., and Asokan, A. (2024). Capsid-mediated control of adeno-associated viral transcription determines host range. Cell Rep. *43*, 113902. https://doi.org/10.1016/j.celrep.2024.113902.
116. Klingler, E., Tomasello, U., Prados, J., Kebschull, J.M., Contestabile, A., Galiñanes, G.L., Fièvre, S., Santinha, A., Platt, R., Huber, D., et al. (2021).

Temporal controls over inter-areal cortical projection neuron fate diversity. Nature *599*, 453–457. https://doi.org/10.1038/s41586-021-04048-3.

117. Bayer, S.A., and Altman, J. (1987). Directions in neurogenetic gradients and patterns of anatomical connections in the telencephalon. Prog. Neurobiol. *29*, 57–106. https://doi.org/10.1016/0301-0082(87)90015-3.

118. Oberst, P., Agirman, G., and Jabaudon, D. (2019). Principles of progenitor temporal patterning in the developing invertebrate and vertebrate nervous system. Curr. Opin. Neurobiol. *56*, 185–193. https://doi.org/10.1016/j.conb.2019.03.004.

119. Baumann, N., Wagener, R., Javed, A., Abe, P., Lopes, A., Lavalley, A., Fuciec, D., Magrinelli, E., Fièvre, S., and Jabaudon, D. (2023). Regional differences in progenitor consumption dynamics shape brain growth during development. Preprint at bioRxiv. https://doi.org/10.1101/2023.08.21.553891.

120. Erclik, T., Li, X., Courgeon, M., Bertet, C., Chen, Z., Baumert, R., Ng, J., Koo, C., Arain, U., Behnia, R., et al. (2017). Integration of temporal and spatial patterning generates neural diversity. Nature *541*, 365–370. https://doi.org/10.1038/nature20794.

121. Hoskins, S.G. (1990). Metamorphosis of the amphibian eye. J. Neurobiol. *21*, 970–989. https://doi.org/10.1002/neu.480210704.

122. Sillar, K.T., Combes, D., Ramanathan, S., Molinari, M., and Simmers, J. (2008). Neuromodulation and developmental plasticity in the locomotor system of anuran amphibians during metamorphosis. Brain Res. Rev. *57*, 94–102. https://doi.org/10.1016/j.brainresrev.2007.07.018.

123. Weiss, L., Segoviano Arias, P., Offner, T., Hawkins, S.J., Hassenklöver, T., and Manzini, I. (2021). Distinct interhemispheric connectivity at the level of the olfactory bulb emerges during Xenopus laevis metamorphosis. Cell Tissue Res. *386*, 491–511. https://doi.org/10.1007/s00441-021-03527-3.

124. Yáñez, J., Eguiguren, M.H., and Anadón, R. (2024). Neural connections of the torus semicircularis in the adult zebrafish. J. Comp. Neurol. *532*, e25586. https://doi.org/10.1002/cne.25586.

125. Gonzalez, A., and Munoz, M. (1987). Some connections of the area octavolateralis pf Pleurodeles waltlii. A study with horseradish peroxidase under in vitro conditions. Brain Res. *423*, 338–342. https://doi.org/10.1016/0006-8993(87)90859-6.

126. Björklund, A., and Dunnett, S.B. (2007). Dopamine neuron systems in the brain: an update. Trends Neurosci. *30*, 194–202. https://doi.org/10.1016/j.tins.2007.03.006.

127. Harris, J.A., Mihalas, S., Hirokawa, K.E., Whitesell, J.D., Choi, H., Bernard, A., Bohn, P., Caldejon, S., Casal, L., Cho, A., et al. (2019). Hierarchical organization of cortical and thalamic connectivity. Nature *575*, 195–202. https://doi.org/10.1038/s41586-019-1716-z.

128. Mano, T., Albanese, A., Dodt, H.-U., Erturk, A., Gradinaru, V., Treweek, J.B., Miyawaki, A., Chung, K., and Ueda, H.R. (2018). Whole-brain analysis of cells and circuits by tissue clearing and light-sheet microscopy. J. Neurosci. *38*, 9330–9337. https://doi.org/10.1523/JNEUROSCI.1677-18.2018.

129. Randlett, O., Wee, C.L., Naumann, E.A., Nnaemeka, O., Schoppik, D., Fitzgerald, J.E., Portugues, R., Lacoste, A.M.B., Riegler, C., Engert, F., et al. (2015). Whole-brain activity mapping onto a zebrafish brain atlas. Nat. Methods *12*, 1039–1046. https://doi.org/10.1038/nmeth.3581.

130. Winnubst, J., Bas, E., Ferreira, T.A., Wu, Z., Economo, M.N., Edson, P., Arthur, B.J., Bruns, C., Rokicki, K., Schauder, D., et al. (2019). Reconstruction of 1,000 projection neurons reveals new cell types and organization of long-range connectivity in the mouse brain. Cell *179*, 268–281.e13. https://doi.org/10.1016/j.cell.2019.07.042.

131. Oh, S.W., Harris, J.A., Ng, L., Winslow, B., Cain, N., Mihalas, S., Wang, Q., Lau, C., Kuan, L., Henry, A.M., et al. (2014). A mesoscale connectome of the mouse brain. Nature *508*, 207–214. https://doi.org/10.1038/nature13186.

132. Kunst, M., Laurell, E., Mokayes, N., Kramer, A., Kubo, F., Fernandes, A.M., Förster, D., Dal Maschio, M., and Baier, H. (2019). A cellular-resolution atlas of the larval zebrafish brain. Neuron *103*, 21–38.e5. https://doi.org/10.1016/j.neuron.2019.04.034.

133. Schindelin, J., Arganda-Carreras, I., Frise, E., Kaynig, V., Longair, M., Pietzsch, T., Preibisch, S., Rueden, C., Saalfeld, S., Schmid, B., et al. (2012). Fiji: an open-source platform for biological-image analysis. Nat. Methods *9*, 676–682. https://doi.org/10.1038/nmeth.2019.

134. O'Rourke, D.P., and Schultz, T.W. (2002). Biology and diseases of amphibians. In Laboratory Animal Medicine (Elsevier), pp. 793–826. https://doi.org/10.1016/B978-012263951-7/50020-X.

135. Yamaguchi, A., Muñoz, M.M., Bose, T.O., Oberlander, J.G., and Smith, S. (2010). Sexually distinct development of vocal pathways in Xenopus laevis. Dev. Neurobiol. *70*, 862–874. https://doi.org/10.1002/dneu.20822.

136. Çiçek, K., Kumaş, M., Ayaz, D., Mermer, A., and Engin, Ş.D. (2011). Age structure of Levant water frog, Pelophylax bedriagae, in Lake Sülüklü (Western Anatolia, Turkey). Basic Appl. Herpetol. *25*. https://doi.org/10.11160/bah.11012.

137. Başkale, E., Ulubeli, S.A., and Kaska, Y. (2018). Age structures and growth parameters of the Levantine frog, Pelophylax bedriagae, at different localities in Denizli, Turkey. Acta Herpetol. https://doi.org/10.13128/acta_herpetol-21026.

138. Kuehn, E., Clausen, D.S., Null, R.W., Metzger, B.M., Willis, A.D., and Özpolat, B.D. (2022). Segment number threshold determines juvenile onset of germline cluster expansion in Platynereis dumerilii. J. Exp. Zool. B Mol. Dev. Evol. *338*, 225–240. https://doi.org/10.1002/jez.b.23100.

Please cite this article in press as: Jaeger et al., Adeno-associated viral tools to trace neural development and connectivity across amphibians, Developmental Cell (2024), https://doi.org/10.1016/j.devcel.2024.10.025

STAR★METHODS

KEY RESOURCES TABLE

REAGENT or RESOURCE	SOURCE	IDENTIFIER
Antibodies		
Chicken polyclonal anti-GFP	Abcam	ab13970; RRID: AB_300798
Rabbit polyclonal anti-GFP	Abcam	ab290; RRID: AB_303395
Goat anti-GFP conjugated to FITC	Abcam	ab6662; RRID: AB_305635
Mouse monoclonal anti-HuC/D (Elavl3/4)	Invitrogen	A-21271; RRID: AB_221448
Rabbit polyclonal anti-RFP	Rockland	600-401-379; RRID: AB_2209751
Mouse monoclonal anti-NeuN	Sigma-Aldrich	MAB377; RRID: AB_2298772
Donkey anti-Mouse IgG (H+L), Cy5	Jackson ImmunoResearch	715-175-151; RRID: AB_2340820
Donkey anti-Chicken IgY (IgG) (H+L), AF488	Jackson ImmunoResearch	703-545-155; RRID: AB_2340375
Goat anti-Rabbit IgG (H+L), AF594	Invitrogen	A-11037; RRID: AB_2534095
Goat anti-Rabbit IgG (H+L), AF488	Abcam	ab150077; RRID: AB_2630356
Goat anti-Mouse IgG (H+L), AF546	Invitrogen	A-11003; RRID: AB_2534071
Bacterial and virus strains		
AAV1-hSyn-EGFP	Gift from Bryan Roth, University of North Carolina at Chapel Hill	Addgene viral prep #50465-AAV1
AAV2-hSyn-EGFP	Gift from Bryan Roth, University of North Carolina at Chapel Hill	Addgene viral prep #50465-AAV2
AAV5-hSyn-EGFP	Gift from Bryan Roth, University of North Carolina at Chapel Hill	Addgene viral prep #50465-AAV5
AAV9-hSyn-EGFP	Gift from Bryan Roth, University of North Carolina at Chapel Hill	Addgene viral prep #50465-AAV9
AAV1-CAG-EGFP	Gift from Bryan Roth, University of North Carolina at Chapel Hill	Addgene viral prep #37825-AAV1
AAV5-CAG-EGFP	Gift from Edward Boyden, Massachusetts Institute of Technology	Addgene viral prep #37825-AAV5
AAV9-CAG-EGFP	Gift from Edward Boyden, Massachusetts Institute of Technology	Addgene viral prep #37825-AAV9
AAVrg-CAG-EGFP	Gift from Edward Boyden, Massachusetts Institute of Technology	Addgene viral prep #37825-AAVrg
AAV-PHP.eB-CAG-EGFP	Gift from Edward Boyden, Massachusetts Institute of Technology	Addgene viral prep #37825-PHPeB
AAV-PHP.eB-CAG-tdTomato	Gift from Edward Boyden, Massachusetts Institute of Technology	Addgene viral prep #59462-PHPeB
AAV-PHP.eB-hSyn-EGFP	CLOVER center	N/A
AAVrg-CAG-tdTomato	Gift from Edward Boyden, Massachusetts Institute of Technology	Addgene viral prep #59462-AAVrg
AAV-PHP.eB-CAG-jGCaMP8s	Neurotools Vector Core	N/A
AAV-PHP.eB-mDlx-NLS-mRuby2	Neurotools Vector Core	N/A
AAV-PHP.eB-CAG-hM4D-mCherry	Neurotools Vector Core	N/A
Chemicals, peptides, and recombinant proteins		
DAKO Mounting medium	Agilent	23023
Normal Goat Serum	Abcam	ab7481
Fluoromount-G Mounting Medium	Invitrogen	00-4958-02
Fluoromount-G Mounting Medium	SouthernBiotech	0100-01
PVA Mounting Medium with DABCO	Millipore Sigma	10981
Fast Green FCF	Sigma-Aldrich	F7252
Leibovitz L-15 Medium w/L-Glutamine, Calcium-Free	US Biological	L2101-02-10L

(*Continued on next page*)

Please cite this article in press as: Jaeger et al., Adeno-associated viral tools to trace neural development and connectivity across amphibians, Developmental Cell (2024), https://doi.org/10.1016/j.devcel.2024.10.025

Continued

REAGENT or RESOURCE	SOURCE	IDENTIFIER
EdU (5-ethynyl-2'-deoxyuridine)	Invitrogen	A10044
2-methylbutane	Sigma-Aldrich	M32631
KwikSil Silicone Adhesive	World Precision Instruments	KWIK-SIL
Paraformaldehyde	Electron microscopy sciences	15710
Methanol	Acros organics	326950010
Hydrogen peroxide	Sigma	216763-500ml
SSCT 20X	Fisher Scientific	15-557-044
Hybridization buffer	Molecular Instruments	N/A
Wash buffer	Molecular Instruments	N/A
Amplification buffer	Molecular Instruments	N/A
DEPC (diethyl pyrocarbonate)	Sigma-Aldrich	D5758
DCM (dichloromethane)	Sigma-Aldrich	34856
DAPI	Sigma-Aldrich	D9542-1MG
Critical commercial assays		
Click-iT™ EdU Kit AF647	Invitrogen	C10340
Experimental models: Organisms/strains		
Pleurodeles waltl	Columbia University	N/A
Xenopus laevis, pigmented	ISTA	N/A
Xenopus laevis, albino	ISTA	N/A
Xenopus laevis, pigmented	Xenopus Express	N/A
Pelophylax bedriagae	Wild caught, Israel	N/A
Oligonucleotides		
PHP-CAG-GFP mFISH-HCR probes	Integrated DNA Technologies	This study; Table S4
Slc17A7 mFISH-HCR probes	Integrated DNA Technologies	This study; Table S4
HCR Amplifier B1-647	Molecular instruments	N/A
HCR Amplifier B2-488	Molecular instruments	N/A
Recombinant DNA		
CAG-EGFP	Gift From Fred Gage, Salk Institute	Addgene plasmid #16664
Software and algorithms		
Fiji 2.14.0	Schindelin et al.[133]	https://fiji.sc/
FactoMineR (RStudio 4.3.2)	Lê et al.[91]	https://CRAN.R-project.org/package=FactoMineR
Prism 10	Graphpad Software, Inc.	https://www.graphpad.com/features
ZenBlue 3.7	Carl Zeiss Microscopy	N/A
Imaris 9.9.1	Oxford Instruments	https://imaris.oxinst.com/
Other		
Nanoject III Programmable Injector	Drummond	3-000-207
PicoSpritzer injection setup	World Precision Instruments	PV820
Electric capillary beveler	Narishige	EG-400
Automatic capillary puller	Sutter Instrument	P-97
Glass capillaries	Drummond	3-000-203-G/X
18 Well Chamber Slides	Ibidi	81816
Nylon suture kit size 5-0	Ethicon	V2130H

EXPERIMENTAL MODEL AND STUDY PARTICIPANT DETAILS

Pleurodeles waltl were obtained from breeding colonies established at Columbia University. Animals were maintained in an aquatics facility at 20-25°C under a 12L:12D cycle.[19] All experiments were conducted in accordance with the NIH guidelines and with the approval of the Columbia University Institutional Animal Care and Use Committee (IACUC protocol AC-AABF2564). Experiments

Please cite this article in press as: Jaeger et al., Adeno-associated viral tools to trace neural development and connectivity across amphibians, Developmental Cell (2024), https://doi.org/10.1016/j.devcel.2024.10.025

were performed with post-metamorphic juvenile (<12 months old) and adult (>12 months old)[19] male and female salamanders, and stage 41 and 50/51 larvae (staged according to[56]).

Albino and pigmented *Xenopus laevis* tadpoles and frogs were either bred and raised at the Institute of Science and Technology Austria (ISTA), or obtained from Xenopus Express and raised at the University of Utah. They were maintained in frog facilities with the water temperature of 18-22°C under a 12L:12D cycle. For larval serotype screening, albino and pigmented tadpoles NF stage 40-60 (staged according to[59]) were used for experiments. For juvenile serotype screening, pigmented post-metamorphic animals, stages 0 to 5 (determined according to[89]), were used. For injections into adults, frogs were defined as adult animals when they were sexually mature, as established by post-mortem examination of gonads and detection of sexually dimorphic features.[134] As an additional correlate of sexual maturity that has been previously established,[135] we also reported weight of each animal in Table S2. All experiments were performed in accordance with the local ethics committee guidelines and the University of Utah Institutional Animal Care and Use Committee (protocol number 2020-0.762.370, 2022-0.137.228, 2024-0.019.606, and 00001947).

Pelophylax bedriagae tadpoles and post-metamorphic frogs (>3 years old as determined by snout-to-vent length and weight measurements[136,137]) were caught in the wild and maintained in a frog facility at 24°C under a 12L:12D cycle. Tadpoles stage 24-27[65,66] were used for experiments. All animal procedures were performed in accordance with the guidelines of the Tel Aviv University ethical committee (animal license TAU-LS-IL-2112-19-4 and TAU-LS-IL-2403-109). Animals were collected under the Israel Nature And National Parks Protection Authority approval (2021/42935).

METHOD DETAILS

Intracerebroventricular, intraspinoventricular, and intraparenchymal injection in Xenopus tadpoles

Xenopus laevis tadpoles stage NF40-60 were anesthetized in 0.01% MS-222 and placed on a piece of gauze in a plastic Petri dish. FastGreen was mixed with AAV prep received from Addgene at a ratio of 1:5 for visualization of injection. Glass capillaries (3-000-203-G/X, Drummond) were pulled at a capillary puller (P-97, Sutter Instrument), their tips trimmed using a fine forceps and beveled at 30 degrees using an electric capillary beveler (EG-400, Narishige). The virus mix was loaded into glass capillaries right before injection using a GelLoader Pipette tip. The capillary was mounted onto a PicoSpritzer injection setup (PV820, WPI) using a piece of tubing while ensuring proper air seal. The PicoSpritzer was switched to gated injection mode. The drop size was normalized using the axioscope eyepiece scale at 2x zoom, setting it to 4-5 lines, approximately 10 nL per drop (per manufacturer's conversion chart). Using a micromanipulator, the needle was inserted into the midbrain ventricle through the skin at the level of midline, into the spinal canal through the dorsal trunk muscle, or into the spinal parenchyma depending on the type of injection. The animals were injected with 4 pumps of virus mix equal to approx. 40-60 nL and the successful injection was confirmed by green coloring of the ventricular space. The injected tadpoles were then returned to a tank with fresh 0.1xMMR solution. 21 days after injection, the animals were sacrificed, dissected, and fixed for 1.5 hours on ice in 4% PFA/PB. The fixed tissue was washed 3 times with ice cold 1xPBS and cryoprotected shaking overnight at 4°C in 15% sucrose-PBS solution complemented with 8% cold fish skin gelatine. The following day, the tissue was lightly dried, embedded in cryomolds filled with tissue freezing medium and frozen in 2-methylbutane (M32631-2.5L, Sigma-Aldrich) on dry ice. 40 μm cryosections were cut at a cryostat (Bright). Sections were imaged on an LSM800 confocal microscope (Zeiss), each had 30-40 optical planes with 1.5 μm steps. The images were stitched using ImarisStitcher, and image processing including contrast adjustment, size filtering (in case of autofluorescent debris), and maximum intensity projection, was done in Fiji.

Intracerebroventricular injection in Pleurodeles larvae

Larvae were deeply anesthetized in 0.02% MS-222 and stabilized in a Sylgard mold. FastGreen was added to AAV aliquots (as provided by AddGene) at a ratio of 1:6 for visualization of the injection site. Glass capillary needles were pulled and then broken open using fine forceps (needle tip diameter ranging 5-15 um), backfilled with mineral oil, and then connected to a Nanoject III injection system (Drummond) and filled with AAV solution. The needle was inserted through the skin, in the lateral telencephalic ventricle of the right hemisphere and 80 nL of virus solution at stage 41, and/or 120 nL at stage 51 was pressure injected (5 nL/sec). For serotype testing, larvae were sacrificed 23 days later and either heads were fixed overnight at 4°C in 4% PFA/PBS, or brains were dissected and also fixed overnight. Heads/brains were then washed in PBS. Heads were cryoprotected in 30% sucrose/PBS and embedded in Tissue-Tek OCT compound (Sakura). 20 μm coronal sections were cut on a cryostat and mounted on glass slides. Brains were processed using a vibratome, generating 70 μm thick floating sections. For detection of the viral DNA/RNA, larvae were perfused 1, 3 or 21 days after injection with PBS-DEPC, brains were dissected and fixed overnight at 4°C in 4% PFA/PBS-DEPC. Brains were then dehydrated (40%, 60%, 80%, 100%, 100% methanol in PBS-DEPC, 15 min each) and incubated in 100% DCM overnight at RT, washed in 100% methanol and stored at -20°C until further processing.

Intracerebroventricular injection in Pelophylax bedriagae tadpoles

Tadpoles were anesthetized in 0.05% MS-222 and placed on a piece of gauze in a plastic Petri dish. AAV viral vectors mixed with FastGreen for visualization (ratio 1:5) were injected using a PicoSpritzer (Cat. num. PV820, WPI) through pulled (P-30 puller, Sutter Instrument) glass capillaries (Cat. num. 3-000-203-G/X, Drummond) trimmed at their end. Injections were into the rostral brain ventricle. Injections contained ~40 nL (injected in 4 puffs) and were confirmed by green coloring of the ventricular space. After injection, tadpoles were returned to their tank and sacrificed after 21 days. Brains were dissected and fixed for 4-12 hours at 4°C in 4%

PFA/PBS. The fixed tissue was washed 3 times with 1xPBS and cryoprotected overnight at 4°C in 15% sucrose-PBS solution complemented with 8% cold fish skin gelatine. The following day, the tissue was lightly dried, embedded in cryomolds filled with tissue freezing medium and frozen in 2-methylbutane (Cat. num. M32631-2.5L, Sigma-Aldrich) on dry ice. 40 μm cryosections were cut at a cryostat (Leica CM1950) and stained using immunohistochemistry.

Intrapallial injections in Xenopus juveniles and adults

Pigmented juvenile *Xenopus* frogs were deeply anesthetized and wrapped in MS-222 soaked gauze to keep them moist. Pigmented adult Xenopus laevis frogs were injected with MS-222 (0.5mL, 1.3%), and wrapped in a wet paper towel. The region of interest was exposed, the craniotomy was performed using a dental drill (Foredom for juveniles, Osada for adults) equipped with a 0.75 mm carbide drill bit (Stoelting) for juveniles or 1.4mm bit (Optimum Dental Supply) for adults, and the meninges were removed using fine forceps. FastGreen was mixed with AAV prep received from Addgene at a ratio of 1:5 for the visualization of the injection site. Glass capillaries were pulled at a capillary puller (P-97, Sutter), their tips trimmed using fine forceps for juveniles or pulled to 10um diameter for adults, and beveled at 30 degrees using an electric beveler (EG-400 for juveniles, and EG-40 for adults, Narishige). The beveled capillaries were backfilled with mineral oil, mounted to a Nanoject III injection setup (Drummond), and loaded with virus mix. 100 nL or 200 nL (see Table S2 for the complete dataset) of AAV solution was then pressure injected into dorsal telencephalon at an injection rate of 1 nL/12 sec, 2 nL/12 sec, 2 nL/6 sec, or1nL/sec, for a total injection time of approx. 20 min. After the injection, the needle was left in the tissue for 5 minutes for juveniles, and 10 minutes for adults to prevent leakage. The skin was sutured using a nylon suture kit size 5-0 (V2130H, Ethicon) for juveniles, and vicryl suture size 6-0 (J489G, Ethicon) for adults. Twenty-one days after injection, the animals were sacrificed, the brains dissected out, and fixed overnight at 4°C in 4% PFA/PB for juveniles and in 4% PFA/PBS for adults. The fixed tissue was washed 3 times with ice cold 1xPBS and cryoprotected shaking overnight at 4°C in 15% sucrose-PBS solution complemented with 8% cold fish skin gelatin for juveniles. Adult fixed brains were transferred to 30% sucrose-PBS solution overnight at 4°C, or until they sank to the bottom of the tubes. For juveniles, the following day, the tissue was lightly dried, embedded in cryomolds filled with tissue freezing medium and frozen in 2-methylbutane (M32631-2.5L, Sigma-Aldrich) on dry ice. For adults, tissue was embedded into 10% gelatin, 30% sucrose, then placed in 4% PFA and 30% sucrose in PBS overnight. 40 μm cryosections were cut at a cryostat (Bright) for juveniles and freezing sliding microtome (American Optical) for adults. Sections were imaged on an LSM800 (juveniles) or LSM 700 (adults) confocal microscope (Zeiss), each had 30-40 optical planes with 1.5 μm steps. The images were stitched using ImarisStitcher (juevniles) and Zeiss Zen Black (adults), and image processing including contrast adjustment, size filtering (in case of autofluorescent debris), and maximum intensity projection, was done in Fiji. The expression strength of adult injections was scored in Table S2, with each animal receiving a score from 0-4. 0 meant that there was no labeling; 1 meant that up to 5 cells were labeled per section around the putative injection site; 2 meant that 6-10 cells were labeled per section; 3 meant that 11-30 cells were labeled per section; and 4 meant that over 30 cells were labeled per section.

Intrapallial injections in post-metamorphic Pleurodeles

Post-metamorphic salamanders were deeply anesthetized in 0.1% MS-222. Heads were stabilized throughout surgery and viral injection using a stereotaxic device equipped with custom-built soft ear cups (Kopf Instruments), and animals were kept moist using 0.1% MS-222 soaked gauze. Craniotomies were performed over a region of interest using a dental drill (Foredom) equipped with a 0.75 mm carbide drill bit (Stoelting), and meninges were removed using fine forceps. FastGreen was added to AAV aliquots (as provided by AddGene or NeuroTools) at a ratio of 1:5 for visualization of the injection site. Glass capillary needles were pulled and then broken open using fine forceps (needle tip diameter ranging 5-15 um), backfilled with mineral oil, and then connected to a Nanoject III injection system (Drummond) 100-200 nL of AAV solution was then pressured injected into neural tissue at an injection rate of 1 nL/12 sec, for a total injection time of approx. 20-40 min. After injections were complete, the needle was left in the tissue for 3-5 min to prevent leakage, after which the craniotomy was covered with a flexible polymer (PDMS) coverslip, and the skin flap was replaced and sealed with KwikSil (World Precision Instruments). Tissue was perfused and harvested 21-25 days after injection, and fixed overnight at 4°C in 4% PFA/PBS. 70 μm floating sections were then cut on a vibratome, and stained using immunohistochemistry.

EdU injections in *Xenopus* tadpoles

EdU administration was performed after intracerebroventricular and/or intraspinoventricular injections of AAV (described above). Anesthetized tadpoles we placed on a moist gauze with the ventral side facing up. A beveled needle was introduced into the peritoneal cavity, and EdU solution was injected (50 mg/kg of body weight). The quantification of overlap between EdU and AAV signal was performed in Imaris on 3D image stacks, each 40 μm thick. The counts were entered into Prism where the plots were generated and statistics calculated as described in Figure legends.

EdU injections in *Pleurodeles* larvae

Deeply anesthetized larvae were placed on their back in a Sylgard mold after intracerebroventricular injection of the AAV virus. EdU was administered intraperitoneally (50 mg/kg of total body weight), using a glass capillary needle and pressure injection.

Please cite this article in press as: Jaeger et al., Adeno-associated viral tools to trace neural development and connectivity across amphibians, Developmental Cell (2024), https://doi.org/10.1016/j.devcel.2024.10.025

Staining protocols

Immunohistochemistry on frozen Xenopus sections

Juveniles. Frozen sections were mounted on glass slides and allowed to dry overnight at 4°C. The tissue was then rehydrated with 1xPBS+0.2%Triton (PBST) for 2-5 minutes. Following another PBST wash, the tissue was left to incubate with chicken anti-GFP (1:500, Abcam ab13970) and mouse anti-HuC/D (Elavl3/4) (1:500, Invitrogen A21271) in PBST overnight at 4°C in a humidified chamber. On the following day, sections were moved to room temperature, washed 3 x PBST, and allowed to incubate in Donkey Anti-Chicken IgY conjugated to Alexa 488 (703-545-155, Jackson ImmunoResearch) and Donkey Anti-Mouse IgG conjugated to Cy5 (1:500; 715-175-151, Jackson ImmunoResearch) with DAPI (1:500) in PBST for 45 minutes at RT. Sections were then washed 3 x PBST and once in 1xPBS to remove unbound antibody. EdU staining was performed on sections of the tadpole that received an EdU pulse, by incubating the sections in the Click-iT reaction cocktail for 1 hour according to manufacturers' instructions (C10340, Invitrogen). Slides were mounted in PVA DABCO antifade medium (10981, Sigma) and left to cure covered for 1 hour at RT. Images were acquired at either a confocal microscope (Zeiss LSM800) or a spinning disk (Nikon CSU W1) using a 20x objective, and processed in Fiji. The quantification of overlap between AAV and Elavl3/4 signal was performed in Image J or Imaris on 3D image stacks, each 40 μm thick. The counts were entered into Prism where the plots were generated and statistics calculated as described in Figure legends.

Adults. Frozen sections mounted on glass slides were rehydrated with 1X PBS for 10 to 20 minutes, followed by incubation with 1X PBS + 0.05% Triton for 10 to 20 minutes. The sections were incubated with goat anti-GFP conjugated to FITC (1:250, Abcam ab6662) in PBST at room temperature on a shaker for 4 hours. The sections were rinsed 3 times with PBST, incubated with DAPI (1:500) in PBST for 10 minutes at RT, and rinsed once with PBST. When sections were dry, slides were mounted with PVA DABCO anti-fade medium (Sigma). The sections were imaged with a LSM700 confocal microscope (Zeiss) with a 20X objective, and processed in Fiji.

Immunohistochemistry on frozen and floating Pleurodeles sections

Frozen sections on glass slides were placed in a humidified chamber, while floating sections were placed in 1 mL of solution in 12-well plates. All sections were blocked at RT for 30 mins - 1 hr in blocking buffer (2.5% BSA, 2.5% sheep serum, 50 mM glycine in PBST (PBS with 0.2% Triton)), and then incubated with chicken anti-GFP (1:500, Abcam ab13970), and/or rabbit anti-RFP (1:5000, rockland 600-401-379) in primary Ab solution (10 mM glycine, 0.1% H2O2 in PBST) overnight at 4°C. Sections were washed 5 x 15 min in PBST at RT, then incubated in Donkey Anti-Chicken IgY conjugated to Alexa 488 (1:500, Jackson ImmunoResearch) and/or Goat Anti-Rabbit conjugated to Alexa 594 (1:500, Fisher) with DAPI (1:1000) in PBST for 2 hrs at RT. Sections were washed 5 x 15 min in PBST at RT and slides were mounted in DAKO fluorescent mounting medium (Agilent Technologies). EdU staining was performed on sections from larvae that received an EdU pulse, after immunohistochemistry, by incubating the sections in the Click-iT reaction cocktail for 45 mins according to manufacturers' instructions (Invitrogen C10340). Images were acquired using a confocal microscope (Zeiss LSM800) and processed in Fiji.

Immunohistochemistry on frozen Pelophylax bedriagae sections

Frozen sections were mounted on glass slides and allowed to dry overnight at 4°C. The tissue was then rehydrated with 1xPBS+0.5% Triton (PBST) for 5 minutes. Following another 3 PBST washes, all sections were blocked at RT for 1 hr in blocking buffer (10% Normal Goat Serum (NGS, ab7481) in 0.3% PBST), and then incubated at 37°C with Anti-GFP (1:1000, ab290) in blocking solution. Sections were washed 5 x 5 min in 0.1% PBST at RT, then incubated Goat Anti-Rabbit IgG H&L (Alexa Fluor 488)(1:500, ab150077) for 45 min at 37°C. Following another 3 x 5 min 0.1% PBST washes, the slices were carefully dried and covered with Fluoromount-G with DAPI (Invitrogen Cat. Num 00-4959-52) and covered by coverslip. Images were acquired using a confocal microscope (3i Marianas Spinning Disc).

Scoring AAV expression in larval screening

For serotype screening in *Pleurodeles* larvae, one section every 140 μm was imaged (single confocal plane). GFP+ cells were counted in the injected hemisphere in the telencephalon, and the average number of GFP+ cells per section was calculated. A score was then applied as such: none (0 cells), low (0.1-10 cells), moderate (11-20 cells), and high (more than 20 cells). For serotype screening in *Xenopus* tadpoles, multiple sections from the telencephalon, diencephalon, and mesencephalon were imaged, each containing 30-40 planes 1.5 μm apart, and a maximum intensity projection was generated in Fiji. Brain images were scored as such: none (0 cells in every section), low (0.1-10 cells per section), moderate (11-20 cells per section), and high (more than 20 cells per section). For serotype screening in *Pelophylax* larvae/tadpoles, each section was stacked acquiring 20-40 images with a 1 μm gap between each image and processed in Fiji. Brain images were scored as such: none (0 cells in every section), low (0.1-5 cells per section), moderate (6-10 cells per section), and high (more than 10 cells per section).

Whole mount Hybridization Chain Reaction (HCR) in situ *hybridization*

HCR-3.0-style probe pairs against the viral DNA/RNA and against *Slc17A7* mRNA were designed using the insitu_probe_generator[138] and ordered from IDT. Brains stored at -20°C in methanol were equilibrated to 4°C and bleached overnight in 5% H_2O_2 in methanol at 4°C. The next day, brains were washed in methanol 2 hrs at RT, incubated two times in HCR wash buffer (Molecular Instruments) until the samples sank, and pre-hybridized in hybridization buffer (Molecular Instruments) for 1 hr at 37°C. Afterwards, brains were incubated 3x overnight at 37°C in probe hybridization buffer with 6 pmol probe for the viral DNA/RNA (45 probe pairs), and 3 pmol probe for *Slc17A7* (33 probe pairs). Excess probe was removed by 3 x 45 min washes in probe wash buffer at 37°C, and 3 x 45 min washes in 5x SSCT at RT. In case of EdU detection, brains were incubated in the Click-iT reaction cocktail for 45 mins according to manufacturers' instructions (Invitrogen C10340) at this step, and washed in 5x SSCT for 10 min. The brains were then preamplified for 2 hrs at 4°C in amplification buffer (Molecular Instruments), and incubated 3x overnight in amplification buffer

with snap-cooled hairpins (60 pM, Molecular Instruments) at 4°C. GFP primary antibody was also added during amplification when necessary. Excess hairpin was removed by 2x 1 hr washes in 5x SSCT and 2x 1hr and one overnight wash in 500 mM Tris-HCl pH7.0. Secondary antibody against the chicken-anti GFP is added during the overnight Tris-HCl wash. The next day, brains were embedded in 4% agarose in Tris-HCl, and 70 μm vibratome slices were made. For the detection of NeuN or Elavl3, these sections were incubated in Tris-HCl buffer with primary antibody (1:500) 2x overnight, washed 3x 15 min in Tris-HCl and incubated in Tris-HCl buffer with secondary antibody (1:500) for 2 hrs at RT and washed again 3x 15 min in Tris-HCl. Sections were then incubated in DAPI in Tris-HCl for 30 min and mounted in DAKO (Agilent) or Fluoromount-G® Mounting Medium (SouthernBiotech). Images were acquired using a confocal microscope (Zeiss LSM800) and processed in Fiji.

Analysis of variable injection outcomes in post-metamorphic Pleurodeles using factor analysis for mixed data (FAMD)

To analyze injection outcomes as a function of measurable variables in an expanded *Pleurodeles* post-metamorphic injection dataset, injection metadata were compiled for experiments that were not restricted to the AAV-GFP construct that was used for screening. This expanded dataset included injections of the following AAV constructs: AAV-PHP.eB-CAG-tdTomato (Addgene #59462-PHPeB), AAV-PHP.eB-CAG-GCaMP8s (Neurotools custom virus), AAV-PHP.eB-CAG-hM4D-mCherry (Neurotools custom virus), AAV-PHP.eB-CAG-EGFP (Addgene #37825-PHPeB), AAV-PHP.eB-mDlx-NLS-mRuby2 (Neurotools custom virus), AAVrg-CAG-tdTomato (Addgene #59462-AAVrg), AAVrg-hSyn-EGFP (Addgene #50465-AAVrg), AAVrg-CAG-EGFP (Addgene #37825-AAVrg), AAV9-CAG-EGFP (Addgene #37825-AAV9), and AAV9-hSyn-EGFP (Addgene #50465-AAV9). Injections of each of these constructs were performed by the same experimenter, using the same injection and floating section immunostaining protocol as described for the serotype screen above. In addition to the weight and age of the animal, injection site, and viral genomes injected, an expression score was assigned to each injected construct. In the case where two constructs were injected in a combined injection solution (dual injection), the outcome for each construct was scored separately (see Table S3 for full dataset).

Injection outcome scores were assigned on a scale from 0-4, based on individual single-plane confocal images of the putative injection site (i.e. where expression was highest). These scores differed from larval injection outcomes described above, due to the higher-intensity, localized labeling induced by direct intraparenchymal injection. Both qualitative and quantitative data were included in score assignment: A score of 0 was assigned if no labeling was observed, 1 was assigned where <10 cells were seen at the injection site, and labeling intensity was low, 2 was assigned where 10-30 cells were seen, and labeling intensity was intermediate, 3 was assigned where 20-50 cells were seen and labeling intensity was high, and 4 was assigned where >50 cells were seen and labeling intensity was high.

To determine differential contributions of injection variables and outcomes, FAMD analysis and plot visualization was performed in RStudio (R 4.3.2) using the FactoMineR software package.[91]

QUANTIFICATION AND STATISTICAL ANALYSIS

Sample sizes (n) are reported in either Tables S1–S3 or the Figure legends. Data are reported as mean ± SEM in all graphs unless otherwise stated. Normality was tested using the Shapiro-Wilk test. For normally-distributed data, differences between groups were assessed using Student's t-test or Analysis of Variance (ANOVA) followed by Tukey's multiple comparisons test when appropriate. For non-normally distributed data, a Kruskal-Wallis test followed by Dunn's multiple comparisons, when appropriate, was performed. Please see Figure Legends for more detail. Statistical analyses were performed in GraphPad Prism and RStudio (R 4.3.2).